Biaxial Response of Individual Bonds in Thermomechanically Bonded Nonwoven Fabrics

Roshelle Wijeratne

Thesis submitted to the faculty of the Virginia Polytechnic Institute and State University in partial fulfillment of the requirements for the degree of

Master of Science
in
Mechanical Engineering

Raffaella De Vita, Co-Chair
David Dillard, Co-Chair
Alexander Leonessa
Amrinder Nain

April 27, 2017
Blacksburg, VA

Keywords: Nonwoven fabrics, Biaxial response, Digital image correlation, Thermomechanical bonds, Strain field maps.

Biaxial Response of Individual Bonds in Thermomechanically Bonded Nonwoven Fabrics

Roshelle Wijeratne

Abstract

Thermomechanically bonded spunbond nonwoven fabrics contain discrete bonds that are formed by melted and fused fibers. Through equi-biaxial tensile testing and simultaneous image capture, the mechanical response of individual bonds was studied through loading in the preferential fiber direction, the machine direction, and in the direction that is perpendicular, the cross direction, of the fabric web. Independent biaxial force and displacement data were collected and analyzed, and the maximum force and stiffness of the bonds in the machine and cross directions were found to be statistically different. After scaling the maximum force and stiffness by a relative basis weight parameter, a fiber orientation parameter, and the width of the bond itself, the peak force and stiffness in the machine and cross directions were found to no longer be statistically different. This indicates that basis weight, fiber orientation, and bond size dictate the biaxial mechanical behavior of the bonds. Furthermore, significant fiber debonding was observed in all the bonds tested, effectively suggesting bond disintegration into the individual component fibers during testing. Digital image correlation, using the captured images, was utilized to calculate local and average Eulerian strains of the bond during the initial stages of the test. The strain experienced by the bonds in the machine direction was always positive and increasing as the biaxial load increased. The strain in the cross

direction, however, experienced increasing and decreasing strain. Local strain maps revealed the highly inhomogeneous strain response of the bonds under biaxial loading.

Biaxial Response of Individual Bonds in Thermomechanically Bonded Nonwoven Fabrics

Roshelle Wijeratne

General Audience Abstract

For numerous industrial and consumer applications, such as the medical, automotive, packaging, and consumer goods, nonwoven fabrics are often thermomechanically bonded at discrete bond locations in patterns appropriate for the intended use. To produce the nonwoven, fibers are extruded onto a belt and the mat of fibers is passed through a calendar roll to form the thermomechanical bonds. As the fibers move on the belt, there is a preferential fiber direction parallel to the belt. Mechanical biaxial tensile tests were performed on nonwoven sheets in order to gain insight into the response parallel and perpendicular to the preferential fiber direction. Force and displacement data were collected and the maximum force and stiffness response parallel to the preferential fiber direction were found to be significantly higher than perpendicular to the preferential fiber direction. Strain measurements were also performed to examine the local strain of the bonds. Knowledge of the biaxial tensile behavior of bonds in nonwovens allows manufacturers to make informed decisions about the ultimate final application of the nonwoven.

Acknowledgements

First and foremost, I would like to acknowledge and give thanks to my co-advisors, Dr. Raffaella De Vita and Dr. David Dillard. They have provided me nothing but support and encouragement over the past 1.5 years. Their combined expertise has taught me not just about succeeding with my research but also how to better succeed outside of school.

I would also like to thank the other researchers in the STRETCH lab. Not only did they provide technical assistance when needed, they also provided countless laughs and moments of relaxation. A special thanks goes to Joe Rittenhouse. I appreciate him teaching me about the project when I first joined, constantly helping with my work and encouraging me, and for being my friend both in and out of the lab.

Furthermore, I would like to thank my committee and other researchers and professors for constant assistance and guidance. Gratitude is also given to the Macromolecule Innovation Institute for providing me opportunities to present my work as well as funding for both the purchase of new equipment and for traveling to a conference.

Last but not least, I would like to thank my family and friends for the constant support.

Table of Contents

Chapter 1. Introduction

Nonwoven fabrics are utilized by numerous industries, including, but not limited to, the automotive, medical, consumer products, and civil engineering industries. Nonwoven fabrics are designed and engineered to provide the required functionality while being a cheaper alternative to woven fabrics [1]. There are different processes to form nonwovens, such as staple, melt-blown, and spunbond. For the spunbond process, the nonwoven fabrics are made from raw pellets that are formed into fibers. These fibers are laid onto a belt in an unorganized fashion and then undergo a bonding process, and occasionally, an additional post-processing treatment. The spunbond nonwoven process is depicted in Fig. 1-1.

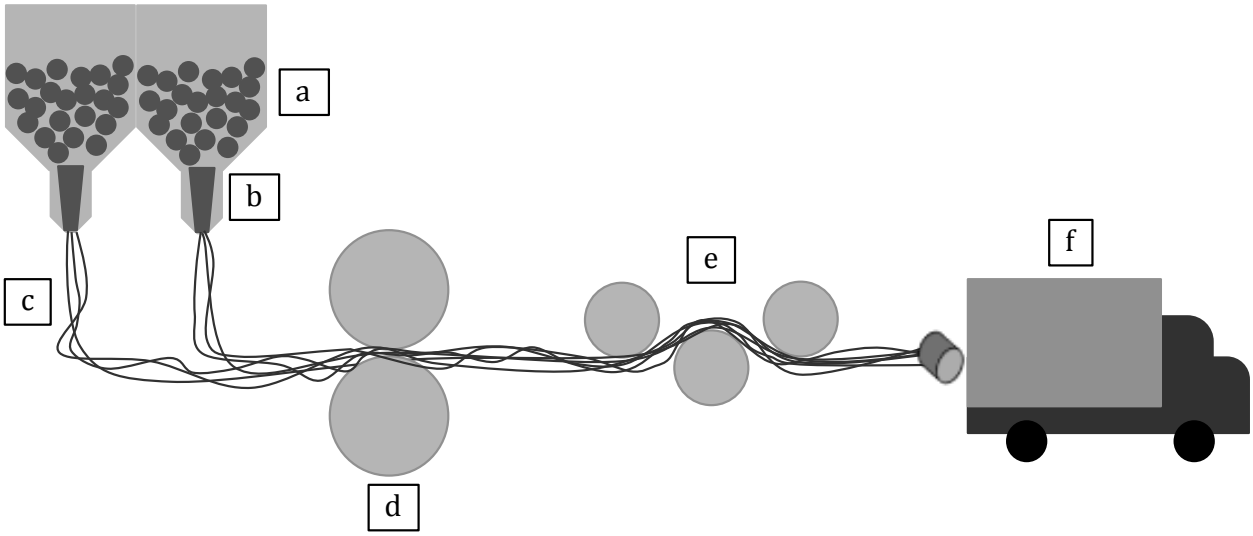

Fig. 1-1 Spunbond nonwoven manufacturing process: (a) the raw pellets are (b) melted and (c) formed into fibers. The fibers undergo a (d) bonding process and an optional (e) post processing prior to being (f) shipped to customers.

In a nonwoven, the fibers comprising it are the mechanical essential element. Fiber characteristics, including polymer type, size, and composition, have been shown to impact the fiber performance, such as tensile strength, in a nonwoven [2]. While in some applications fibers that are homo-filament are used, bi-component hetero-filament fibers

may be more suitable in other applications. Two incompatible polymers, such as polyethylene and polypropylene, are formed together. There are various patterns in which the two polymers can be formed; a common one is sheath-core [3]. The lower melting point polymer, as the sheath, can be melted and used as an adhesive, while the higher melting point polymer, at the core, causes the fiber to retain some of the original integrity.

The crucial component of the manufacturing of a nonwoven is the bonding process. While there are numerous nonwoven bonding treatments, such as chemical and solvent, one common technique is thermomechanically bonding them. This process involves passing a fiber mat through a heated calender roll. The heat will soften the fibers, then nips on the roll will weld the fibers together when they come in contact, forming discrete bonds. These bonds are essential to the nonwoven's stiffness and strength [4]. The thermomechanical bonding process is illustrated in Fig. 1-2. Due to the movement of the fibers along the belt and through the calender roll, there is an associated preferential fiber direction, which is parallel to the direction of the belt. This preferential fiber direction is referred to as the machine direction (MD), while the direction that is perpendicular to the preferential fiber direction is referred to as the cross direction (CD).

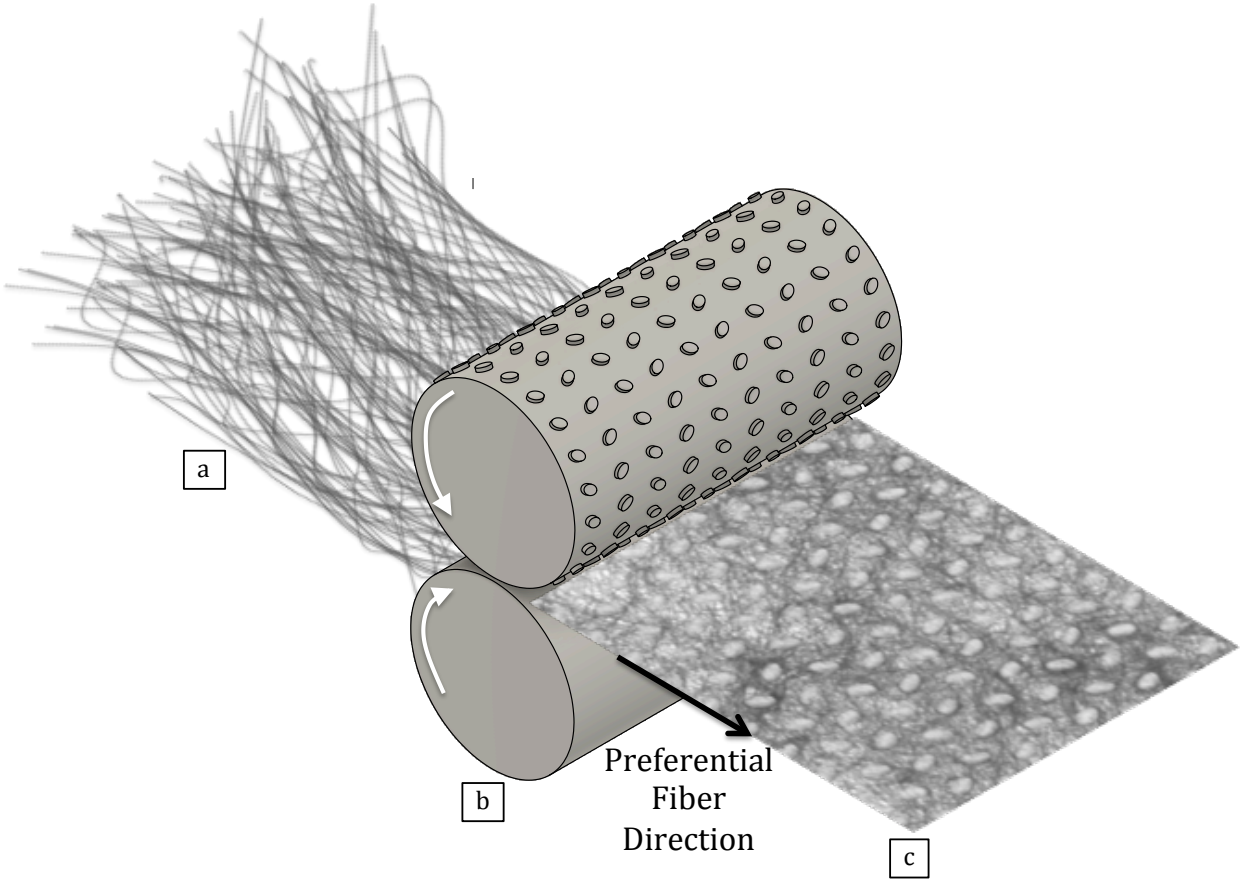

Fig. 1-2 Thermomechanical bonding process where (a) a web of fibrous material is passed through (b) a heated calender roll with nips. The nips melt and weld fibers together, forming (c) discrete bond points.

The organization of the fibers and the discrete bonds lead to highly anisotropic thermo-mechanically bonded nonwoven fabrics [5], which experience unique deformation behavior. In order to gain insight into the deformation response, uniaxial tensile tests are commonly performed on nonwovens. Previous work has predominately focused on testing coupons of nonwovens with dimensions on the order of centimeters. The uniaxial tests performed on nonwovens provide visual and quantitative data that can be used in order to validate finite element models [6-9]. Studies have also performed uniaxial tensile tests in order to compare nonwovens of different polymer compositions. For example, Wang et al.

[10] compared a bicomponent PP/PE (volume ratio of 70/30) nonwoven to a PP nonwoven. Sample strips measure 25 x 75 mm were tested in the machine direction at 300 mm/min. It was found that at failure, the tensile force reached by the PP nonwoven was more than 150% higher than the PP/PE nonwoven; however, the extension reached by the PP/PE nonwoven was approximately 200% higher than the PP no nwoven. While the uniaxial tests were performed on coupons of nonwovens, the deformation of individual bonds within the coupon was also observed, but not quantified. The two nonwovens had varied bond response, with the PP/PE bond being described as "flexible" and the PP as "rigid". Nanjundappa et al. [11] also previously studied individual bonds within a nonwoven coupon, looking at the affect of bonding temperature on the failure mechanism of the individual bond. Similarly, Kim et al. [12], while testing nonwoven coupons bonded at various temperatures, also examined the failure mechanism of individual bonds. The most complete quantitative characterization of individual bonds was performed by Bhat et al. [13]. These authors examined how the bond (e.g., bonding temperature, bond size and area) affected the uniaxial peak load and tear strength of nonwovens by testing small strip specimens (80 mm x 5 mm) in the MD and CD.

Previous biaxial tensile studies have also been performed on nonwoven fabrics, but at a scale larger than an individual bond. Goswami et al. [14] used biaxial tests of nonwovens in order to determine the Poisson's ratio in thermally bonded nonwoven fabrics. Polyester fibers bonded at different bonding temperatures and with varying concentrations of binder were used to create 6 cm by 6 cm specimens. These specimens were tested equi-biaxially at extension rates of 50% and 200% per minute. Similar tests were performed uniaxially. By assuming the elastic behavior of the nonwoven fabrics is orthotropic, it was determined

that biaxial tests, rather than uniaxial tests, provide a more accurate estimate of the Poisson's ratio and is a more appropriate way to determine constitutive properties of nonwoven fabrics.

Digital image correlation (DIC) is a noncontact method for measuring strain. The process involves applying a random paint or speckle pattern to the specimen, performing the desired mechanical test (i.e. uniaxial tensile test) while simultaneously recording images, then tracking the movement of the speckle pattern via computer software and computing the resulting strain. DIC enables the measurement of highly nonlinear and non-homogenous strain fields and has been utilized extensively in measuring the strain of biological materials [15], which also contain fibrous networks. This method has also been applied to nonwoven fabrics. While studying the effects of testing temperature and strain rate on polypropylene nonwoven fabrics, Jubera et al. [16] utilized DIC in order to measure the macroscopic level strains. The fabric was cut to 150 mm by 100 mm rectangular coupons and tested uniaxially at 0.08, 0.8, and 10 mm/s and in testing environments at 298 and 383 K. DIC and the resulting strain maps allowed for the analysis of the onset strain localization. Overall, damage was shown to not be local and diffuse through the sample prior to the maximum load. In addition, Ridruejo et al. [17] performed uniaxial tests on nonwovens at a macroscopic scale (specimens measuring 100 mm x 100 mm) in order to analyze the failure locus and validate a finite element model. DIC was also performed in order to measure the strain experienced by the nonwoven. Additional work was performed by Ridruejo et al. [18] to measure strains through DIC in notched nonwoven specimens being pulled in uniaxial tension.

In order to develop a stronger understanding of the behavior of thermomechanical bonds in nonwoven fabrics, this study will focus on biaxial tests performed on individual bonds. The variation between the response in the MD and the CD will be analyzed, with attempts to scale the responses by considering the relative basis weights, fiber orientation, and bond width. Furthermore, upon the completion of each biaxial test and through subsequent image analysis, strain measurements will be computed through DIC. Using the biaxial force-displacement data and calculated strain estimates, the anisotropy and strain inhomogeneity of the bonds not only will be visually observed, but will also be quantified. This new knowledge is crucial when trying to systematically control the integrity of the bonds during the manufacturing process as well as determining a suitable final application of a nonwoven.

Chapter 2. Materials and Methods

2.1. Specimen Preparation

Commercial spunbond bi-component thermomechanically bonded nonwoven fabric was obtained to test the biaxial properties of individual bonds within the fabric. The fabric was composed of polyethylene/polypropylene sheath-core fibers and had an average weight of 20 gsm (gram per square meter). Prior to mechanical testing, the nonwoven fabric sheet was scanned using an optical transmission scanner (Epson Perfection V850 Pro) at 16-bit grayscale and 2540 dpi (dots per inch) resolution for subsequent image processing to determine local fiber frequency and fiber orientation.

Due to a visible variation in fiber frequency (herein referred to as fiber density) across the nonwoven sheet, a relative basis weight analysis was performed to provide a metric for selecting comparable bonds to test [19]. To calculate the relative basis weight, the scanned images were analyzed in ImageJ software (ImageJ, National Institute of Health) and regions measuring $2\ mm \times 2\ mm$ and centered around individual bonds were analyzed. Relative basis weight is derived from the Beer-Lambert law [20], where the light transmitted, I, is defined by:

$$I = I_o e^{-\mu \rho L}, \tag{1}$$

where I_o, μ, ρ, and L are the incident light, mass-absorption coefficient, density of the substrate, and thickness of the substrate, respectively. In this application, the substrate is the nonwoven fabric. By setting ρL as mass per unit area, or basis weight, B, (1) can be rewritten as:

$$I = I_o e^{-\mu B}, \tag{2}$$

or modified as:

$$B = \frac{1}{\mu}\ln\left(\frac{I_o}{I}\right). \quad (3)$$

While I_o can be measured by taking a light measurement of an area without the nonwoven present and I can be measured by taking a light measurement transmitted through the nonwoven, μ cannot easily be obtained. Therefore, by multiplying by μ, a relative basis weight, B_{rel}, is instead calculated from:

$$B_{rel} = B\mu = \ln\left(\frac{I_o}{I}\right). \quad (4)$$

The relative basis weight is a scalar measurement between 0 and 1, where zero signifies no material present and unity represents complete absorption. This quantity allows for comparing areas within a nonwoven sheet. For example, if region A has a relative basis weight of 0.25 and region B has a relative basis weight of 0.50, it can be concluded that region B has twice as much material present compared to region A. Once a relative basis weight analysis was performed on over 300 randomly chosen bonds, 20 bonds were selected that were within a small range of relative basis weights of one another.

Polyethylene terephthalate glycol (PTEG) sheets having a 0.25 mm thickness (Thick Clear Plastic Sheet, K&S Precision Metals) were cut using a laser cutter (VLS3.60, Universal Laser System) to create mounting frames for biaxial nonwoven cruciform specimens. Details about the mounting frame and its dimensions are illustrated in Fig. 2-1. As shown in Fig. 2-1, the center of the mounting frame featured a $2\ mm \times 2\ mm$ window within which the bond to be tested was centered.

The nonwoven was cut using micro-scissors into cruciform specimen with an arm width of 3 mm and with the arms oriented along the MD and CD. The specimen were

attached to the mounting frame using a double-sided tape (Scotch Double Sided Permanent Tape, 3M) in order to place the bond in the center of the mounting frame, precisely in the square window. Four notches were created on the cruciform specimen outside the $2\ mm \times 2\ mm$ square region along the diagonal directions using micro-scissors. This was done to further reduce the gage length of the square region containing the bond. Using a quick curing epoxy recommended for bonding polyolefins (J-B Weld 50133), the cruciform specimen region outside the square window was completely secured on the mounting frame. By creating the $2\ mm \times 2\ mm$ square window within the mounting frame and using epoxy, the gage length of the nonwoven specimens was reduced to $2\ mm$ in both test directions, and square specimens containing single bonds in their centers were biaxially tested. Fig. 2-2 shows a nonwoven specimen completely adhered to the mounting frame. A random speckle pattern was created on each specimen using an airbrush (Badger 150, Badger Air Brush Co.) with a fine needle (Badger Fine Needle for #100 and #150, Badger Air Brush Co.). In order to achieve approximately $10\ \mu m$ in diameter speckles, India ink (Super Black India ink, Speedball) was sprayed into a $30\ cm \times 20\ cm \times 20\ cm$ chamber, approximately 15-18 cm away from the specimen and the resulting mist settled onto the specimen. The fine random speckle pattern was needed for sufficient resolution in the non-contact DIC strain measurements performed upon the completion of the biaxial test.

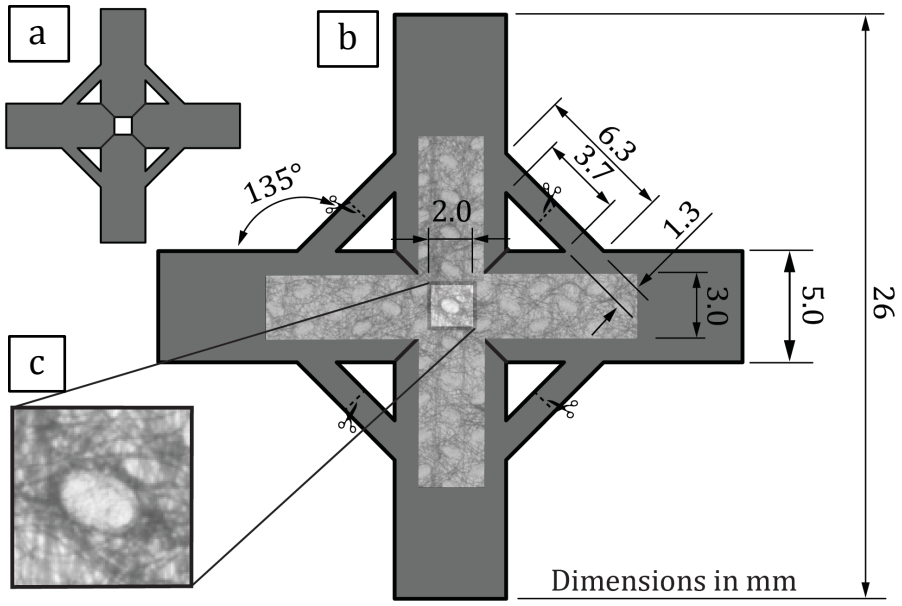

Fig. 2-1 Schematics of the nonwoven specimen over a plastic frame: (a) plastic frame with a $\mathbf{2\times2}\ \boldsymbol{mm^2}$ square window, (b) nonwoven cruciform specimen on plastic frame, (c) bond in the center of the $\mathbf{2\times2}\ \boldsymbol{mm^2}$ square window of the plastic frame

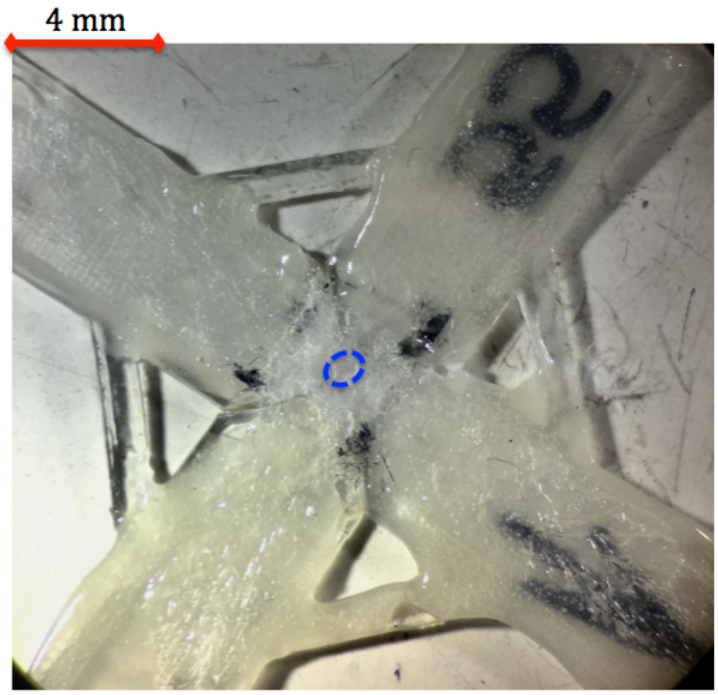

Fig. 2-2 Nonwoven specimen adhered to mounting frame with PSA and epoxy, prior to speckling. The bond to be tested is located in the middle of the cruciform and mounting frame, circled in the blue dashed line.

2.2. Biaxial Tensile Testing

A biaxial tensile testing machine was custom-built for testing the single bonds cut from the nonwoven fabric. Four linear actuators (Linear actuator, 25 mm travel, RS-232 plus manual control, Zaber Technologies Inc.) were used to control the motion along two perpendicular axes. Two 8.9 N (2 lb.) load cells (Jr. Miniature S-Beam Load Cell, FUTEK Advanced Sensor Technology, Inc.) were mounted to two adjacent actuators. Custom-built mechanical clamps with embedded nuts were designed and made using a 3D printer (Replicator, MakerBot). Details about the clamp design are shown in Fig. 2-3. The clamps were then attached to either the actuators or the load cells. In order to collect images of the specimen during biaxial testing, an XGA camera (Stingray F-080, Allied Vision Technologies) equipped with a 0.7X-4.5X lens (VZM 450i Zoom Imaging Lens, Edmund Optics) was used. The complete biaxial tensile test stage, with a specimen loaded for testing, can be seen in Fig. 2-4. A LabVIEW program (LabVIEW, National Instruments) was developed to control the actuators as well as record images of the bond, actuator displacements, and loads during biaxial testing. Furthermore, manual controllers within this program were designed to allow the user to keep the bonds centered in the field of view during testing.

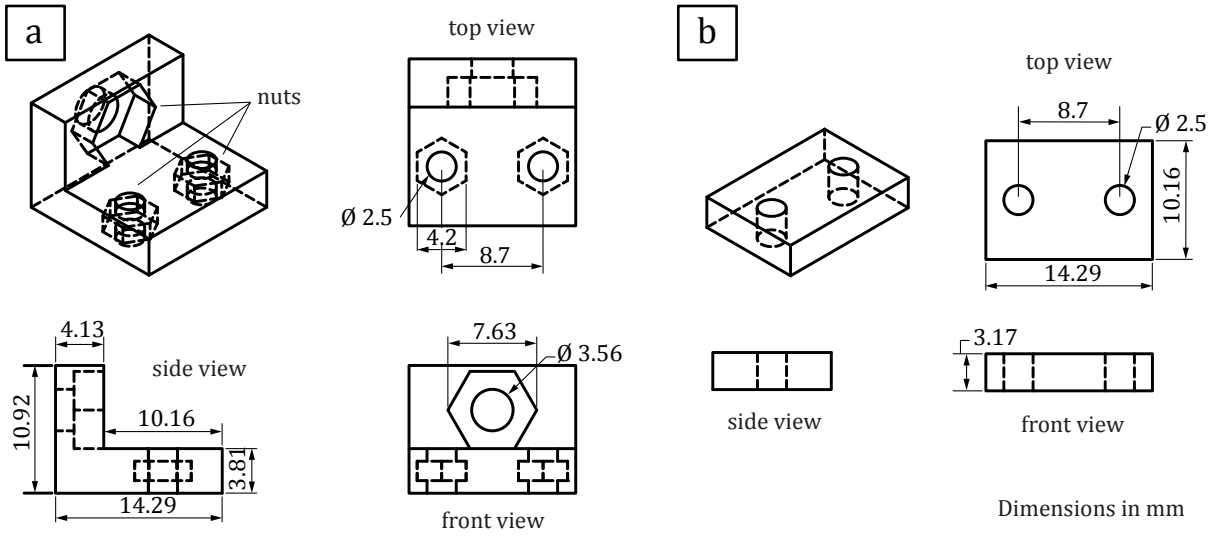

Fig. 2-3 Design of (a) bottom and (b) top portion of the 3D printed clamps.

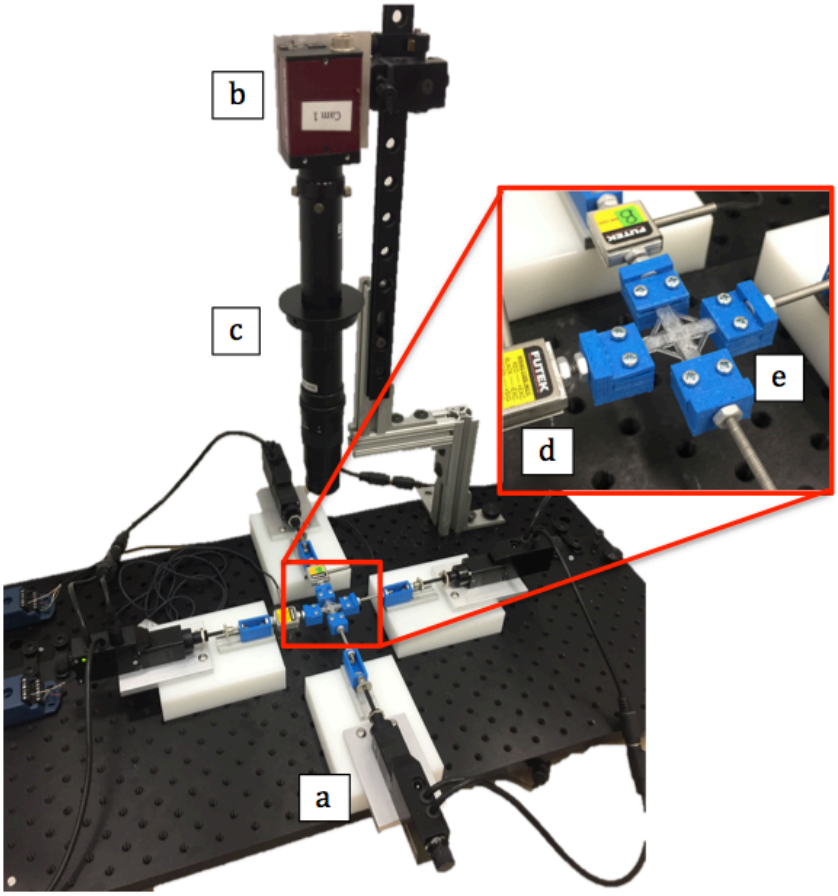

Fig. 2-4 Custom-built tensile test stage with (a) four linear actuators, (b) camera, (c), lens, (d) two load cells, and (e) four 3D printed clamps (shown with specimen loaded for testing).

Equi-biaxial tests were performed at room temperature (20°C) at a constant 0.1 mm/s displacement rate (resulting in a nominal strain rate within the test section of 0.05/s) on n = 20 specimens. Once each cruciform specimen was attached to the clamps, the diagonal braces of the PTEG mounting frame were cut to allow movement of the $2\,mm \times 2\,mm$ central square region of the specimen along the two loading axes. Locations of the cuts to the frame are shown as the scissor marks in Fig. 2-1. The specimen was preloaded to 0.01 N in both loading directions prior to testing. Each specimen was then equi-biaxially stretched until either failure in both directions occurred or one of the actuator's physical travel limit was reached.

2.3. Strain Analysis

Recorded image sequences of each speckled bond within the $2\,mm \times 2\,mm$ central square region of the cruciform specimen were used to calculate the evolving in-plane strain maps using an open source digital image correlation (DIC) software package [21] written in Matlab (Matlab 2016, Mathworks). The software was modified to manually select the speckles and track their motion to calculate the Eulerian-Almansi strain tensor. By tracking the speckle pattern, the displacement field components, u_x and u_y, for the bond were calculated as follows:

$$u_x = x - X \tag{5}$$

$$u_y = y - Y, \tag{6}$$

where X and Y are the coordinates of a generic point in the reference configuration at the pre-load state and x and y are the coordinates of such point in the deformed configuration.

The x- and X- axes are selected to coincide with the MD and y- and Y- axes with the CD of the nonwoven. The in-plane local Eulerian-Almansi strain components e_{xx}, e_{yy}, and e_{xy}, were calculated from:

$$e_{xx} = \frac{1}{2}\left(\frac{\partial u_x}{\partial x} + \frac{\partial u_x}{\partial x} - \left(\frac{\partial u_x}{\partial x}\right)^2 - \left(\frac{\partial u_y}{\partial x}\right)^2\right), \tag{7}$$

$$e_{yy} = \frac{1}{2}\left(\frac{\partial u_y}{\partial y} + \frac{\partial u_y}{\partial y} - \left(\frac{\partial u_x}{\partial y}\right)^2 - \left(\frac{\partial u_y}{\partial y}\right)^2\right), \tag{8}$$

$$e_{xy} = \frac{1}{2}\left(\frac{\partial u_x}{\partial y} + \frac{\partial u_y}{\partial x} - \frac{\partial u_x}{\partial x} \cdot \frac{\partial u_x}{\partial y} - \frac{\partial u_y}{\partial x} \cdot \frac{\partial u_y}{\partial y}\right). \tag{9}$$

Hereafter and throughout the thesis, “strain” will be used to denote the Eulerian-Almansi strain.

In order for this analysis to be executed properly, at each data point, the tracked points first were fitted to an evenly spaced grid. Two meshes were created using the x- and y-displacements and the evenly spaced grid. The gradients of the meshes provided the derivative components necessary to calculate the strain components at every point on the grid; this allowed for a strain map to be generated. This method was previously developed [21], however, modifications were made to calculate the Eulerian-Almansi strain by taking the gradients with respect to the current configuration. In addition, the strain components could be averaged over the gridded region to provide the average e_{xx}, e_{yy}, and e_{xy} for each time step. For consistency, average strain analysis was performed up to 2.3 mm displacement along the MD and CD and used four tracking points.

2.4. Orientation Analysis

The orientation of fibers in the vicinity of the selected bond was calculated using an OrientationJ plug-in [22] for ImageJ. The $2\ mm \times 2\ mm$ regions centered on bonds that were previously used to calculate the relative basis weight of the bonds were used for the orientation calculation. Prior to orientation analysis using the plug-in, the image was first filtered through a Gaussian Blur set to 20 microns, equal to the fiber diameter, to remove fine details. The image was then filtered through a Fourier high-pass filter, with large structures being filtered down to 3 pixels and small structures being filtered up to 1 pixel, in order to accentuate the fibers. The plug-in was used to calculate the fiber orientation, with the structure tensor specification set at 1.5 times the fiber diameter. The structure tensor is a matrix based on the gradient of the image and is a useful tool for detecting edges [23]. Edges were predominately detected in the fibrous regime, as well as at the perimeter of the bond. The interior portion of the bond contained fewer detectable edges due to the fusion of fibers during the bonding process, and therefore, fewer pixel counts were recorded in that area. As such, the orientation data is weighted to fibers in the peripheral region around the bond. The output of the OrientationJ plugin is a count of pixels oriented at each angle from -90° to 89°, in 1° increments.

From the orientation distribution, orientation parameters were calculated for each specimen. The orientation parameter is calculated with respect to the testing direction; the biaxial tests performed have two testing directions, the MD and CD, and therefore two different orientation parameters were required. For the MD orientation parameter, the orientation distribution had 0° aligned with the MD; for the CD orientation parameter, the orientation distribution was shifted so that 0° aligned with the CD. Based on Cox's analysis

of the strength of paper and other fibrous materials [24], the orientation parameter, O_p, was calculated from:

$$O_p = \frac{\int_{-\pi/2}^{\pi/2} f(\theta) \cos^4 \theta d\theta}{\int_{-\pi/2}^{\pi/2} f(\theta) d\theta} \quad (10)$$

where $f(\theta)$ is the orientation distribution. The orientation parameter is a dimensionless quantity with a value between zero and 1.0, where a 1.0 corresponds to perfect alignment in the testing direction and zero indicates perfect perpendicular alignment with the testing direction.

2.5. Force-Displacement Analysis

To calculate the stiffness in the initial linear region of the force-displacement curves, a linear fit of the curves was performed in Matlab. Starting at 0.1 mm displacement, the force-displacement data were fit to the equation of a line over a gradually increasing displacement interval. The linear fit procedure was repeated until the R^2 value of the linear fit dropped below 0.995. The stiffness was defined as the slope of the linear fit. For each specimen, the stiffness was calculated in both the MD and CD.

The width of the bonds was measured in both the CD and MD in ImageJ using the previously scanned images. The widths were taken perpendicular to MD and CD axes and through the center of the bond, as illustrated in Fig. 2-5. In order to scale the stiffness and maximum force, the stiffness and maximum force measurements were divided by the basis weight (BW), orientation parameter (O_p), and width of the bond (w), as shown by:

$$X_{norm} = \frac{X_{raw}}{BW \cdot O_p \cdot w}, \quad (11)$$

where X is either the maximum force or stiffness.

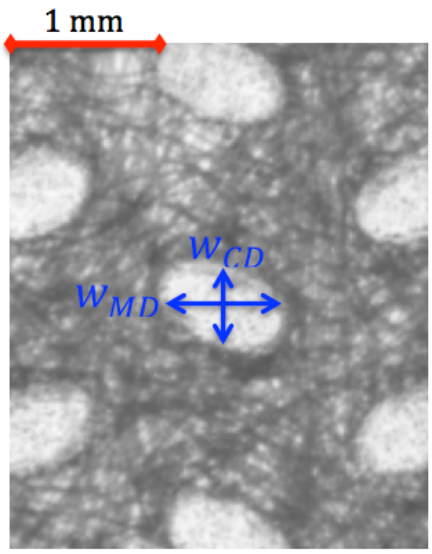

Fig. 2-5 The widths of the bond in the MD and in the CD.

2.6. Statistical Analysis

Means and standard deviations were calculated for the maximum force, displacement at maximum force, stiffness, scaled maximum force, and scaled stiffness (n = 20). The Student's t-test was used to compare the differences between these variables in the MD and CD. The threshold for statistical significance was chosen to be 5%. Statistical analysis was performed in Matlab using the built-in ttest( ), mean( ), and std( ) functions to calculate the p-value, mean, and standard deviation, respectively.

Chapter 3. Results

The bonds (n = 20) that were chosen for testing had a mean relative basis weight of 0.348 ± 0.002 (mean ± standard deviation). The force and displacement biaxial data collected for each of the twenty specimens are divided up into four groups and are presented in Fig. 3-1. The force-displacement curves are characterized by having a linear region at low displacements (<1mm), followed by a nonlinear region in both the MD and CD. In every test, the specimen reached a higher peak force in the MD than in the CD. Following these peak forces, small rises and drops in the force-displacement curves were observed. These likely resulted from the breakage of fibers surrounding the bond. The data were then averaged for each displacement point in order to calculate an average force-displacement curve in the MD and CD (Fig. 3-2). Fig. 3-2 presents the average MD and CD force-displacement curves, in addition to individual force-displacement curves from the specimens. This figure better represents the variation that was recorded among the force-displacement data.

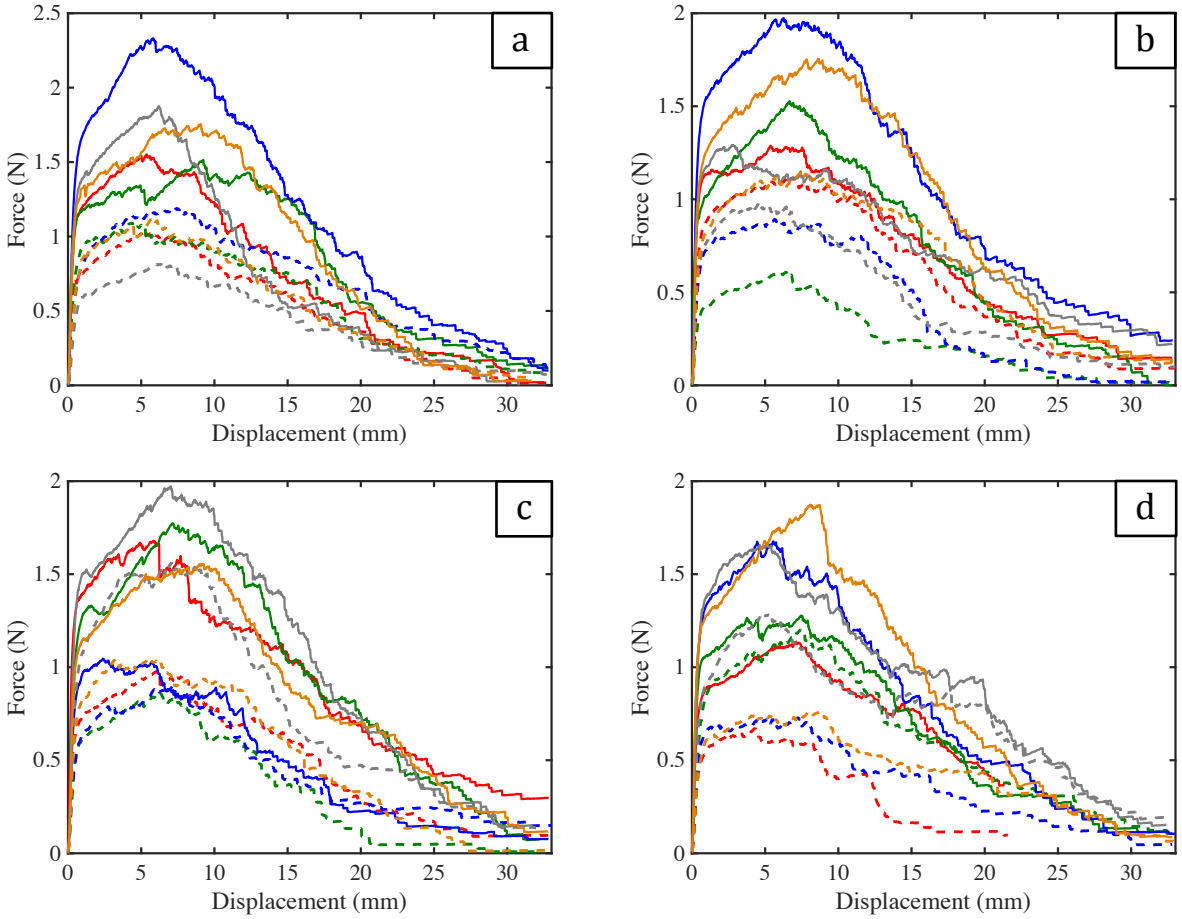

Fig. 3-1 Force-displacement curves for (a) tests 1-5 (b) tests 6-10 (c) tests 11-15 (d) tests 16-20. The solid lines denote the force-displacement data in the MD while the dotted lines in the identical color represent the corresponding force-displacement data in the CD.

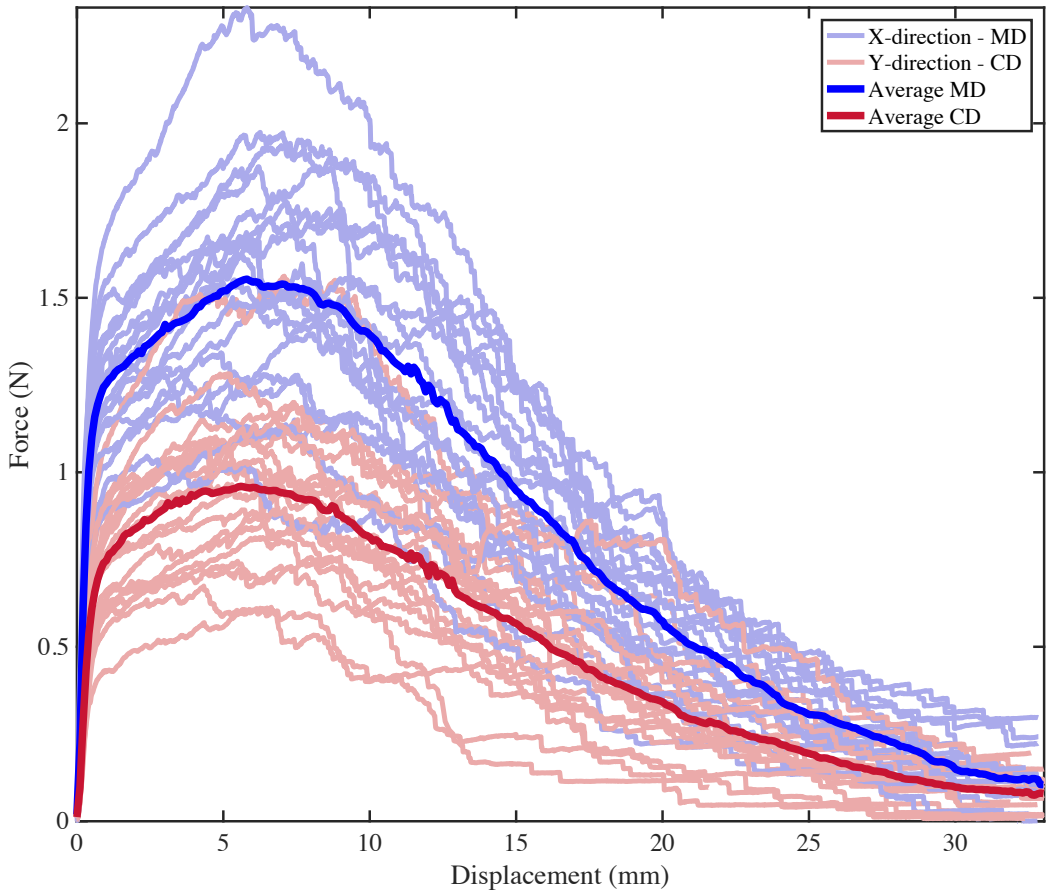

Fig. 3-2 Force-displacement curves from the tested specimens (n = 20) and the average force-displacement curves.

The maximum force reached by each specimen in both the MD and CD was found, as well as the displacement at which the maximum force occurred. The average maximum force in the MD was 1.597 ± 0.316 N, and occurred at a displacement of 6.419 ± 1.840 mm. The average maximum force in the CD was 0.978 ± 0.255 N, and occurred at a displacement of 6.13 ± 1.296 mm. The box plots of the maximum force and displacement at maximum force in the MD and CD are shown in Fig. 3-3. While the maximum force was higher in the MD than it was in the CD, the displacement at which the maximum force occurred was similar in both the MD and CD. A Student's t-test revealed that the difference in the

maximum force in the MD and CD had a statistical significance (p-value = $1.10\times10^{-7} < 0.05$); on the other hand, the difference in the displacement at the maximum force was not statistically significant (p-value = $0.554 > 0.05$).

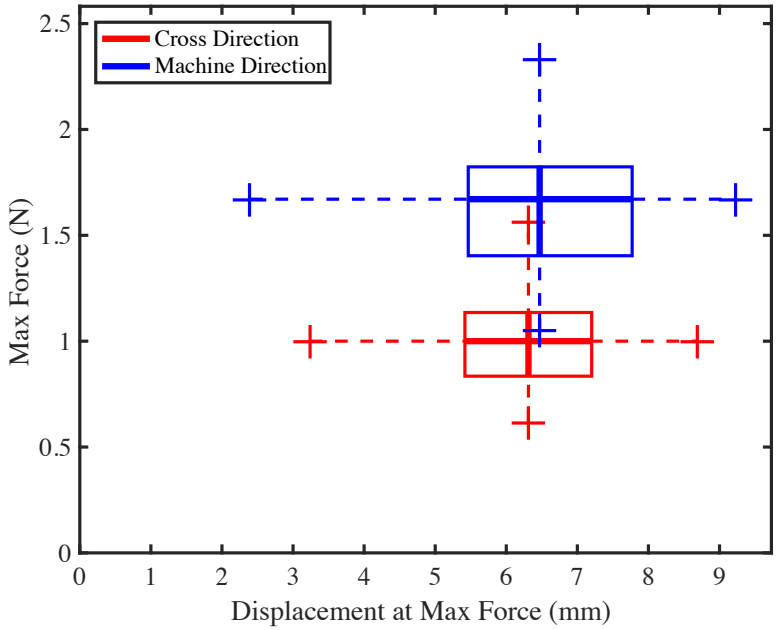

Fig. 3-3 Box plots of the maximum force (N) and displacement (mm) at maximum force with the box representing the 25th and 75th percentiles.

The force-displacement data from 0.0 to 0.8 mm displacement, which contains the initial linear region as well as the onset of the nonlinear region, for the specimens are plotted in Fig. 3-4. The average stiffness of the initial linear region of the force-displacement curve in the MD was 3.570 ± 0.806 N/mm, while in the CD, the stiffness averaged 1.645 ± 0.410 N/mm. Box plots of the stiffness values are shown in Fig. 3-5. The Student's t-test revealed the difference in stiffness values in the MD and CD was statistically significant (p-value = $2.05\times10^{-9} < 0.05$).

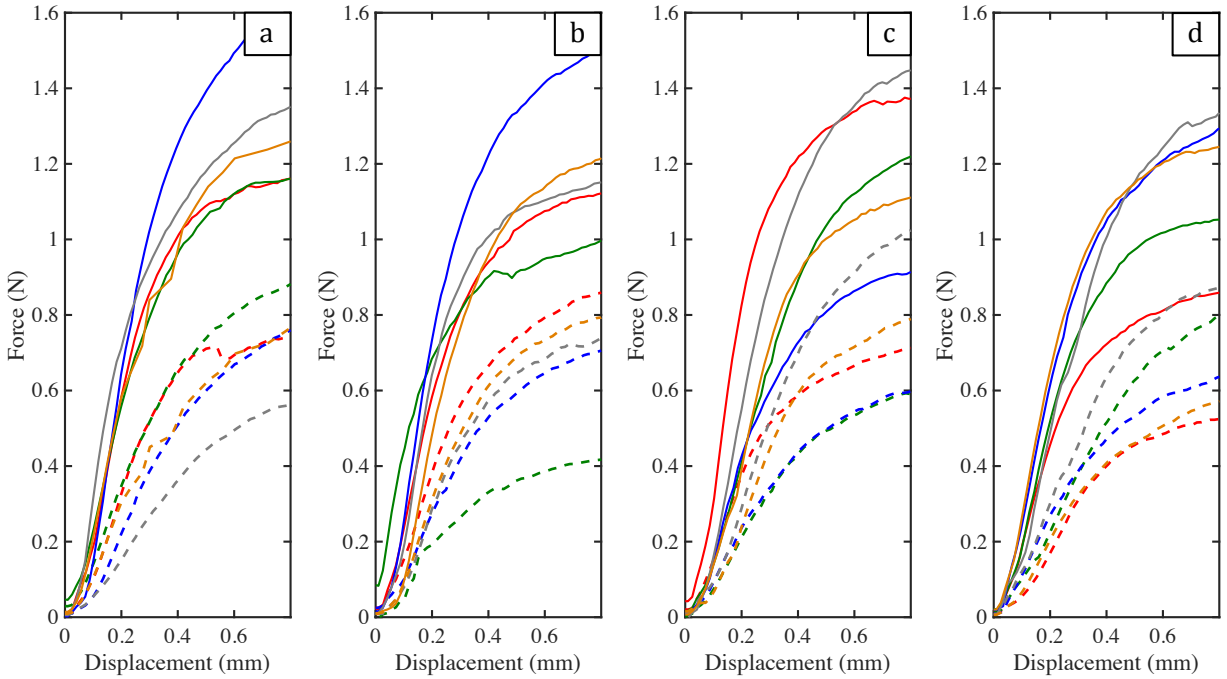

Fig. 3-4 The force-displacement curves, plotted up to 0.8 mm, corresponding to the curves in **Fig. 3-1**. Curve fitting was started at 0.1 mm.

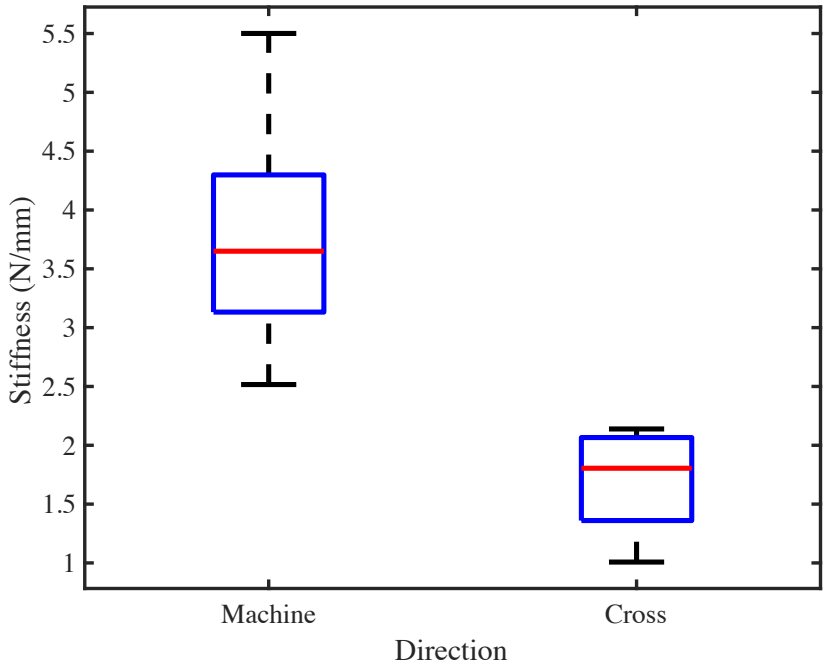

Fig. 3-5 Box plots of the stiffness (N/mm) in the MD and CD, with the box representing the 25th and 75th percentiles.

Fiber orientation of each of the 2 $mm \times 2\ mm$ specimen, containing both the bond and surrounding fibers, was also measured. The fiber orientation frequency (within 1° bins) relative to the MD is shown in Fig. 3-6 for the 20 samples. This figure indicates that the fibers had a varied orientation within each specimen, although in some cases preferred fiber orientation was noted. For example, in Fig. 3-6b, the red orientation frequency curve indicates fewer fibers oriented in the MD compared to the frequency of fibers oriented closer to the CD. When looking at the corresponding red force-displacement curves in Fig. 3-1b, one can note that the force-displacement curve in the CD is similar to one in the MD. On the other hand, the green orientation frequency curve in Fig. 3-6b indicates more fibers oriented in the MD compared to in the CD. The corresponding green force-displacement curves in Fig. 3-1b shows a clear difference in the specimen's mechanical behavior in the MD versus in the CD, with the response in the MD reaching higher forces than in the CD.

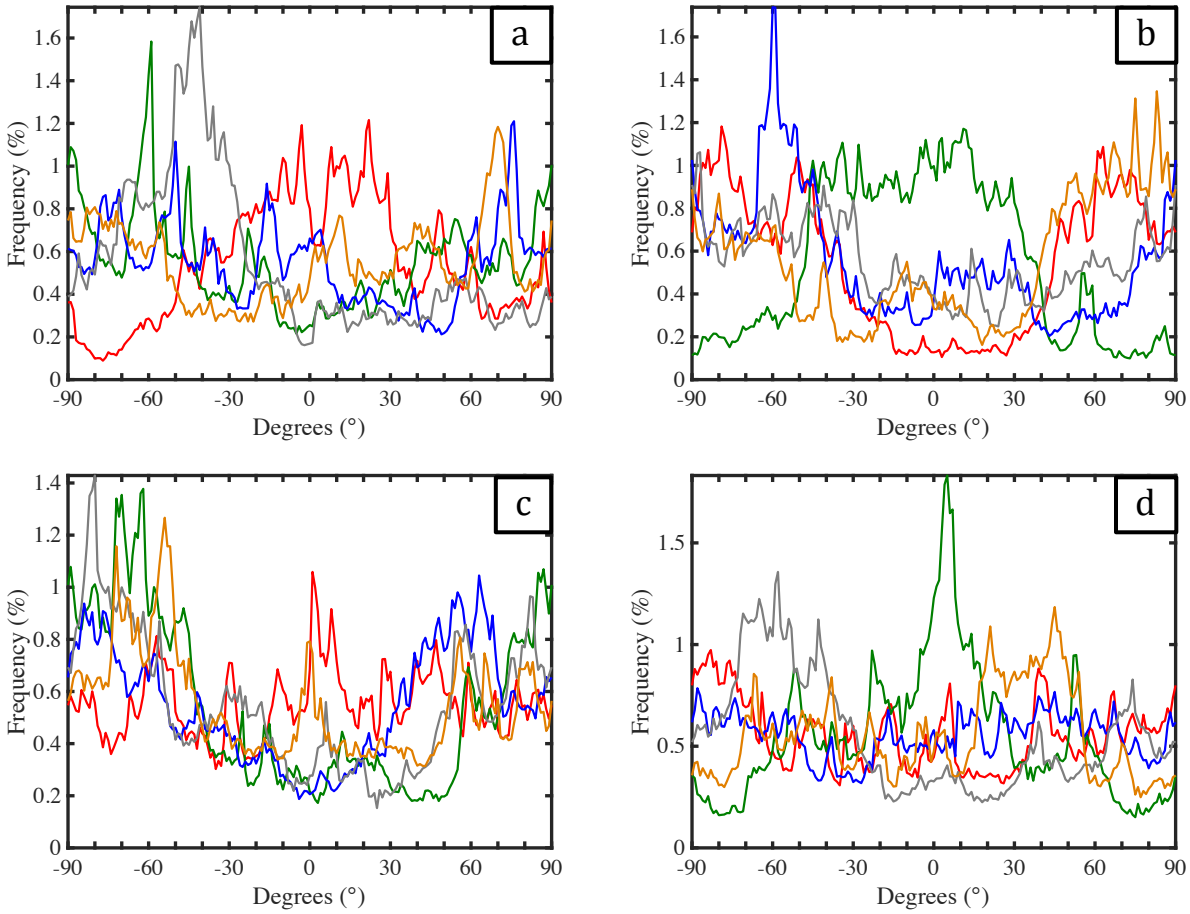

Fig. 3-6 Orientation frequency line graphs for (a) tests 1-5 (b) tests 6-10 (c) tests 11-15 (d) tests 16-20, with colors corresponding to the test's force-displacement curves in **Fig. 3-1**. MD aligns with 0° and CD with 90°.

After calculating the orientation parameters based on the frequency data in Fig. 3-6, the widths of the bond were found. In the CD, the widths ranged from 0.480 to 0.660 mm and in the MD, the widths ranged from 0.693 to 0.833 mm. The calculated stiffness and maximum forces were then scaled by the orientation parameter, basis weight, and width of the bond. The scaled maximum force per unit width in the MD and CD were 16.5 ± 6.36 N/mm and 16.9 ± 7.07 N/mm, respectively. The scaled stiffness per unit width in the MD and CD were 38.3 ± 18.0 N/mm^2 and 29.0 ± 12.1 N/mm^2, respectively. A Student's t-test revealed that the differences in the maximum force per unit width and stiffness per unit

width in the MD and CD were not statistically significant ($p = 0.884 > 0.05$ and $p = 0.144 > 0.05$, respectively). Box plots comparing the maximum force and stiffness with the scaled maximum force and stiffness are presented in Fig. 3-7.

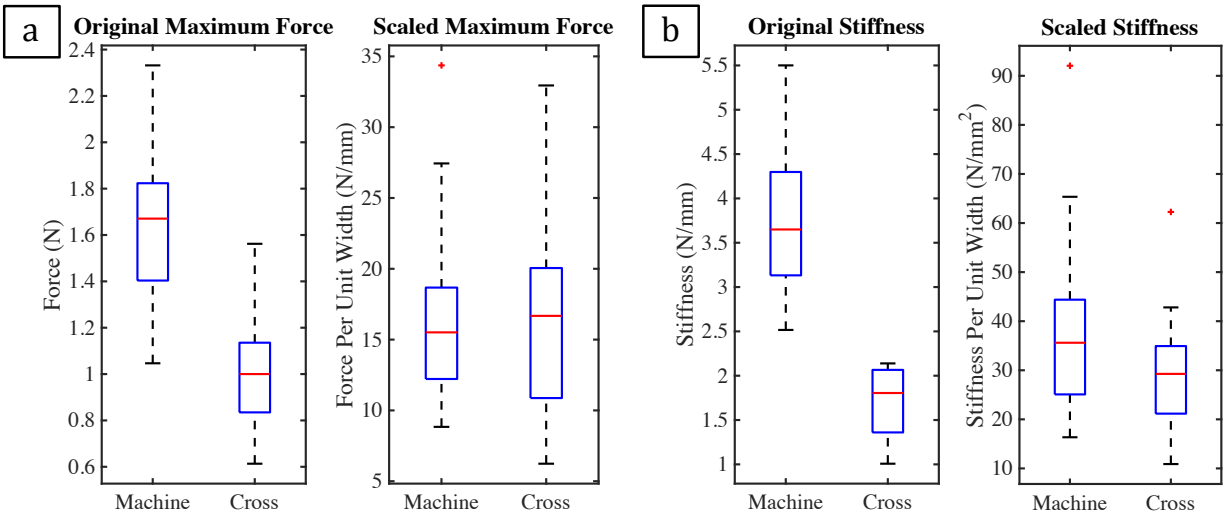

Fig. 3-7 Box plots comparing the original and scaled (a) maximum force and (b) stiffness in the MD and CD. The boxes represent the 25th and 75th percentile. Scaling was performed using the relative basis weight, orientation of fibers, and bond width.

The behavior of the bond was visualized through the images collected during the test. In all of the tests, the bond would disintegrate and return back into a fibrous form, as seen in the photo sequence in Fig. 3-8. These original fibers would be load bearing until fiber failure occurred.

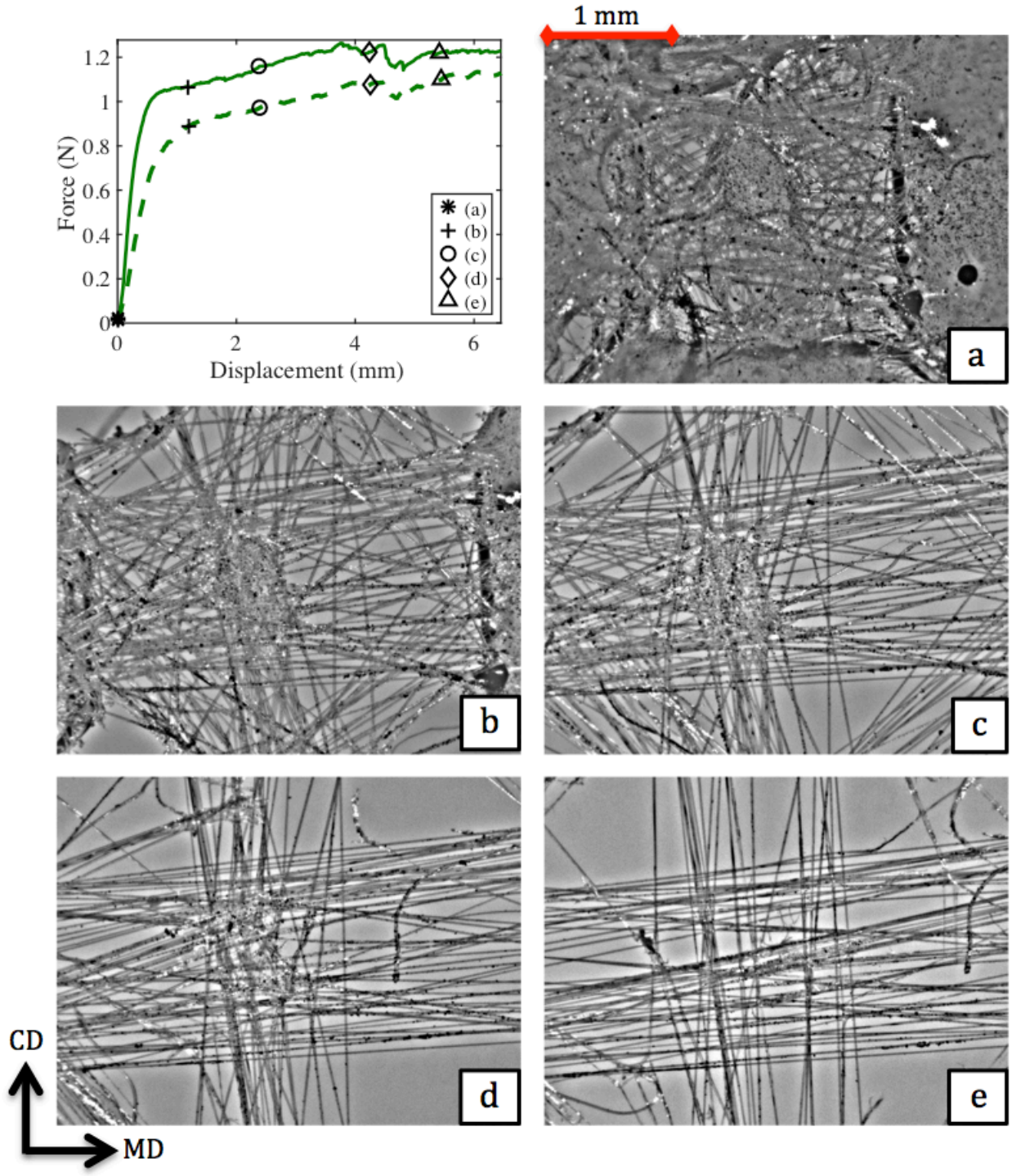

Fig. 3-8 A portion of the force-displacement data of a bond in the MD and CD, corresponding to the green force-displacement curves in **Fig. 3-1**d. A gradual disintegration of a bond can be seen at specimen forces in the MD and CD of (a) 0.021 N and 0.015 N, (b) 1.06 N and 0.890 N, (c) 1.16 N and 0.972 N, (d) 1.22 N and 1.07 N, and (e) 1.22 N and 1.10 N, respectively.

Average strain curves were generated for the entire set of specimens up to 2.3 mm displacement. Some representative force-strain curves are reported in Fig. 3-9. The 2.3 mm displacement was selected based on the images of the specimens that were successfully analyzed using the DIC method. After this displacement, some speckles could not be tracked due to fiber damage and breakage within the bond. The forces at this displacement corresponded with 86.4% ± 4.4% of the maximum force in the MD and 84.3% ± 7.2% of the maximum force in the CD.

The strain in the MD and strain in the CD were plotted against the corresponding forces for some selected specimens (Fig. 3-9). The shear strain was measured but was negligible for most, but not all, specimens. For all the specimens, the strain in the MD increased with load, while the strain in the CD varied between consistently increasing (Fig. 3-9a), consistently decreasing (Fig. 3-9b), and a combination of increasing and decreasing (Fig. 3-9c). The calculated average strain was found to be relatively independent of the points selected for tracking in a limited comparison (0).

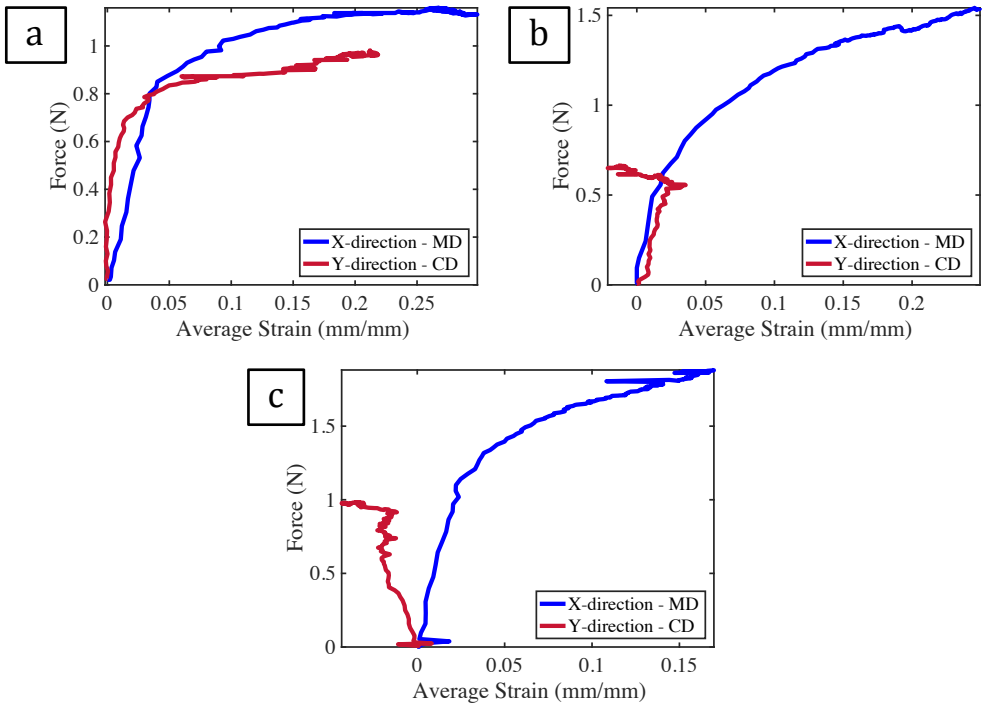

Fig. 3-9 Force versus average strain curves in the MD and CD. While the bonds always experienced positive strain in the MD, in the CD, the bond (a) experienced consistently increasing strain, (b) experienced a change between increasing and decreasing strain, and (c) experienced predominantly decreasing strain.

Strain maps were generated for selected specimens to compute the local (rather than average) strain fields in the MD and CD within the bond. These maps are reported in Fig. 3-10 and Fig. 3-11. In the MD (Fig. 3-10), the overall bond strained but as the specimen approached displacements in the MD and CD of 3 mm, a pronounced tensile strain concentration developed near the top-left region of the bond, indicated by the red region in Fig. 3-10h. The specimen in the CD (Fig. 3-11) experienced minimal strain, but similar to the MD, an area of high compressive strain developed near the top, indicated by the blue region in Fig. 3-11h. Furthermore, the two sets of images demonstrated how the local strain within the bond is non- homogenous.

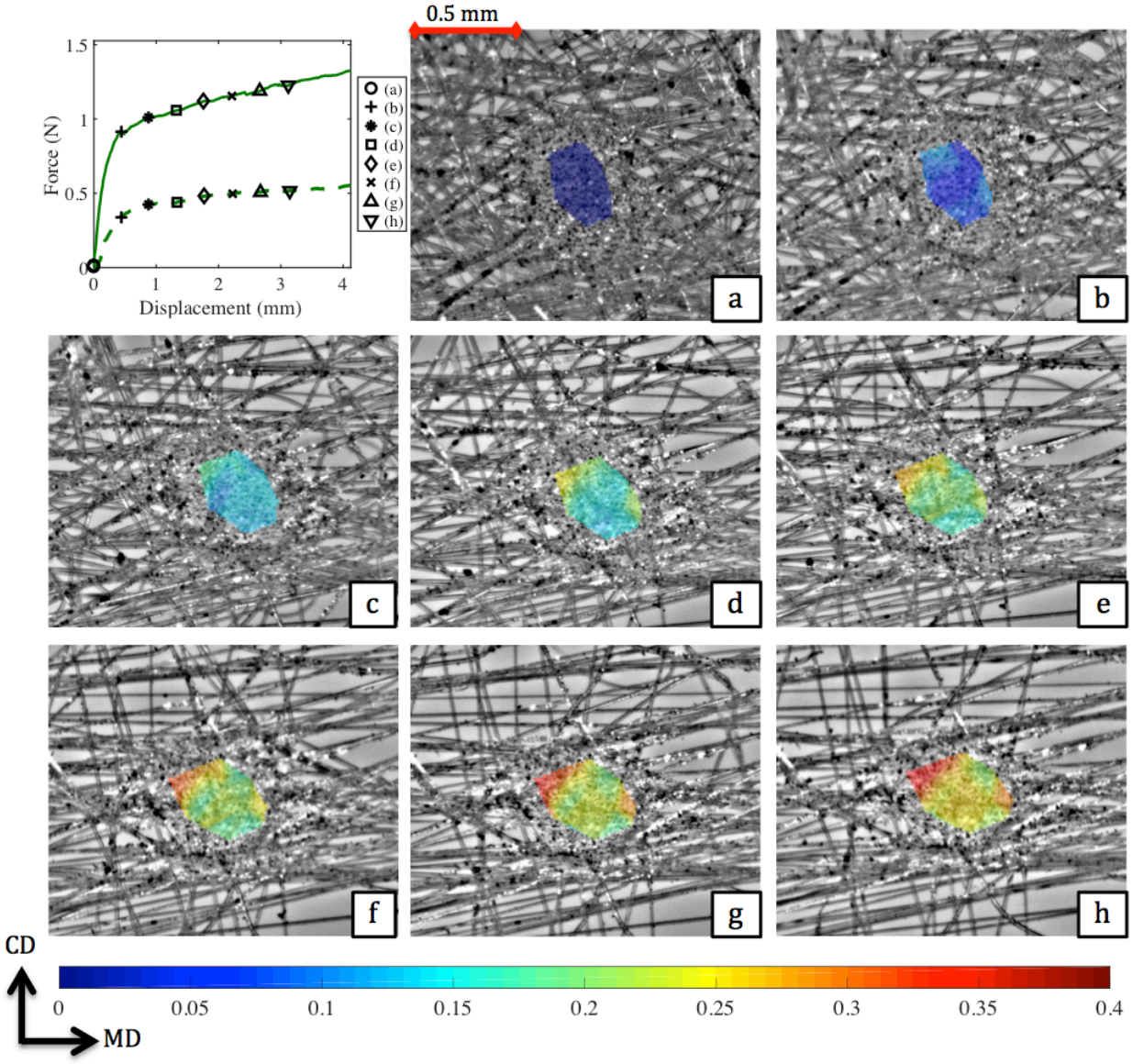

Fig. 3-10 A portion of a specimen's force-displacement curves in the MD and CD, corresponding to the green force-displacement curves in **Fig. 3-1**b. The $\boldsymbol{e_{xx}}$ strain maps (corresponding to strain in the MD) for a specimen at loads in the MD and CD of (a) 0.012 N and 0.011 N, (b) 0.914 N and 0.241 N, (c) 1.02 N and 0.426 N, (d) 1.06 N and 0.440 N, (e) 1.12 N and 0.481 N, (f) 1.16 N and 0.496 N, (g) 1.18 N and 0.501 N, and (h) 1.23 N and 0.517 N, respectively.

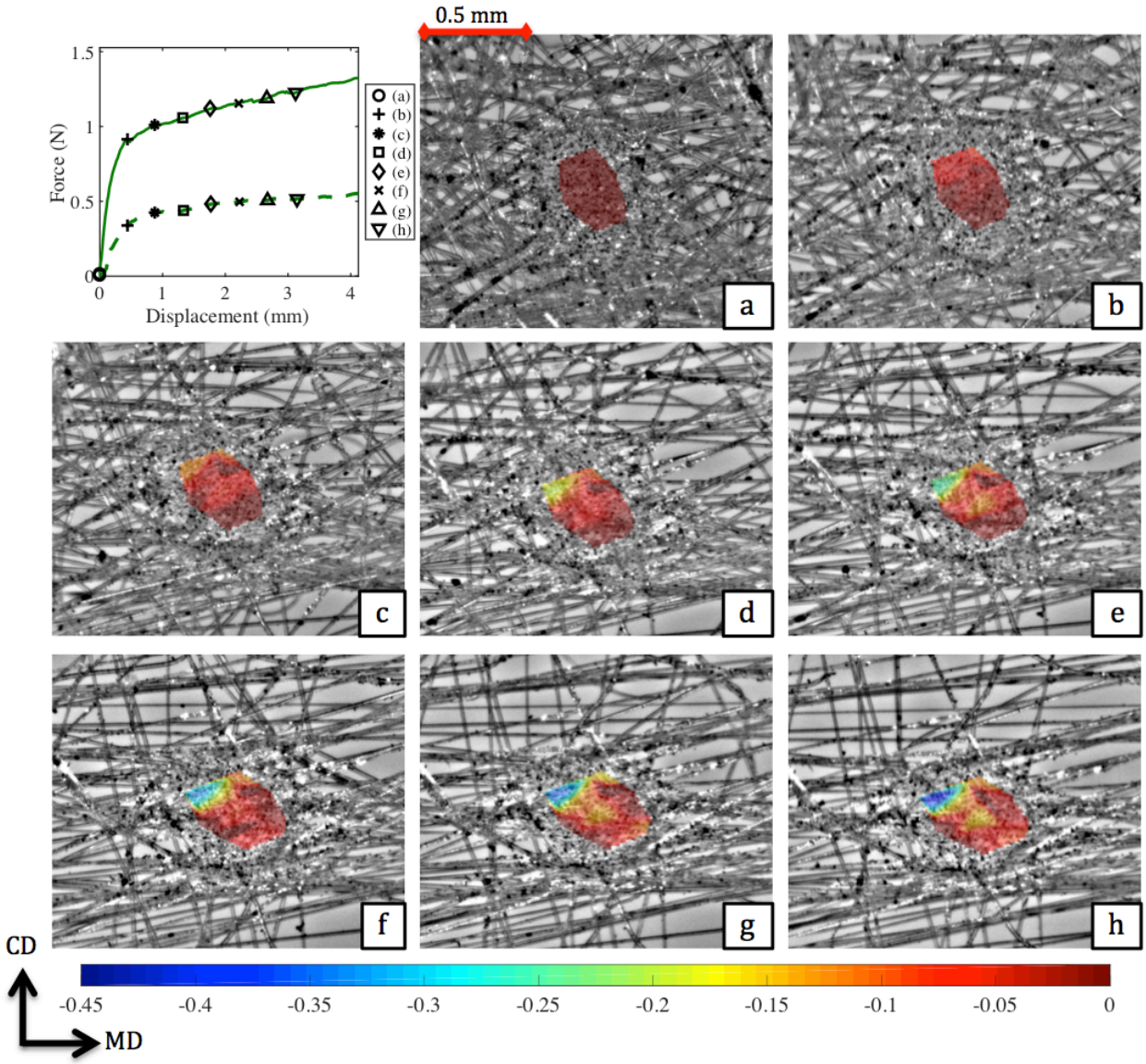

Fig. 3-11 A portion of a specimen's force-displacement curves in the MD and CD, corresponding to the green force-displacement curves in **Fig. 3-1**b. The $\boldsymbol{e_{yy}}$ strain maps (corresponding to strain in the CD) for the same specimen in **Fig. 3-10**, also at loads in the MD and CD of (a) 0.012 N and 0.011 N, (b) 0.914 N and 0.241 N, (c) 1.02 N and 0.426 N, (d) 1.06 N and 0.440 N, (e) 1.12 N and 0.481 N, (f) 1.16 N and 0.496 N, (g) 1.18 N and 0.501 N, and (h) 1.23 N and 0.517 N, respectively.

For one specimen, the bond was observed to shear (Fig. 3-12). By developing the strain maps, the shear strain was found to be significant but was highly localized, occurring

within a small portion of the bond. The shear strain map in the bond can be seen in Fig. 3-12.

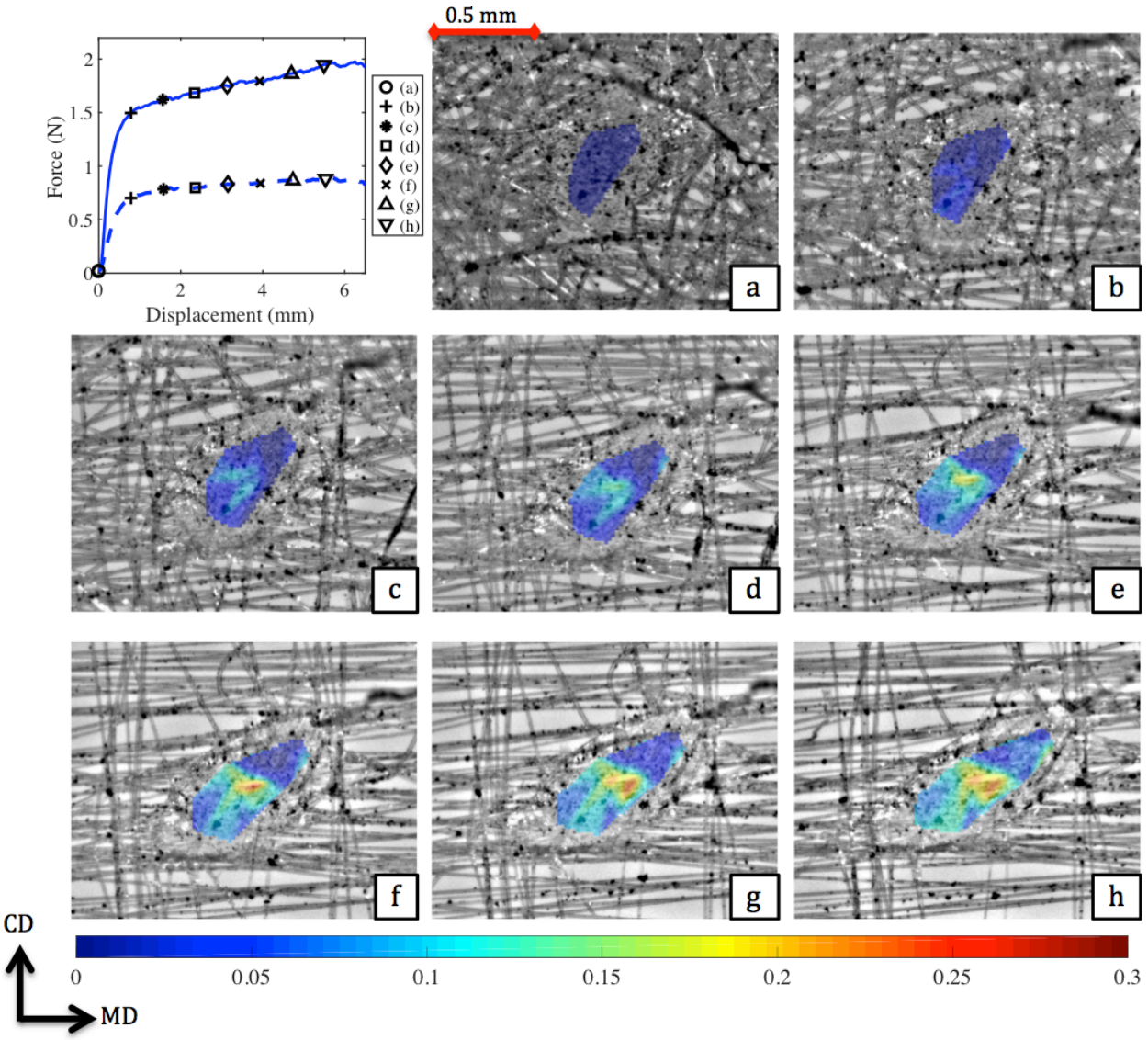

Fig. 3-12 A portion of a specimen's force-displacement curves in the MD and CD, corresponding to the blue force-displacement curves in **Fig. 3-1**b. The e_{xy} strain maps (shear strain) for a specimen at loads in the MD and CD of (a) 0.015 N and 0.014 N, (b) 1.49 N and 0.702 N, (c) 1.62 N and 0.788 N, (d) 1.69 N and 0.799 N, (e) 1.75 N and 0.831 N, (f) 1.79 N and 0.837 N, (g) 1.86 N and 0.869 N, and (h) 1.95 N and 0.882 N, respectively.

Chapter 4. Discussion

This work examined the response of individual bonds in nonwoven fabric subjected to displacement-controlled equi-biaxial tests. A unique, custom-built biaxial tensile test stage with image acquisition for post-processing strain analysis was developed to test the nonwoven specimens containing individual bonds. In addition, a new nonwoven specimen mounting method was presented. By calculating an orientation parameter based on the fibers surrounding the bond, and taking into account the width of the bond and its relative basis weight, the difference between the specimens' maximum force and stiffness in the MD and CD was reduced. Image analysis using the DIC method gave insight into the local and average strain experienced by the bonds.

Clamping the nonwoven for testing individual bonds biaxially was found to be challenging. Trying to directly clamp a $2\ mm \times 2\ mm$ square specimen with a bond in its center was difficult and, therefore, a plastic frame with a $2\ mm \times 2\ mm$ square window was designed to first attach a cruciform specimen (Fig. 2-1). By using an epoxy that is compatible with the polyolefin fibers, the fibers outside of the $2\ mm \times 2\ mm$ square region were secured properly. Several tests were performed in order to verify that significant fiber slippage did not occur at any time during testing. However, this clamping technique could affect the biaxial response of the bond and an in-depth analysis of the effect of different clamping methods should be performed, similar to what has been done on larger specimens of various materials [25-27].

A small preload of 0.01 N was applied to the specimens prior to testing in order to remove as much slack from the fibers as possible as well as ensure that the bond remained in the lens' plane of focus during the test. Despite the application of pre-load, the force-

displacement curves for some specimens still exhibited an initial nonlinear region, indicating that the fibers were not fully straightened at the beginning of the test. This can be expected due to the varied waviness of each fiber. For this reason, when computing the stiffness of the specimens from the force-displacement curves, the initial displacement for this computation was selected so that all the curves were linear. A sample of a force-displacement curve with a toe region followed by the region used for the stiffness calculation is presented in Fig. 4-1.

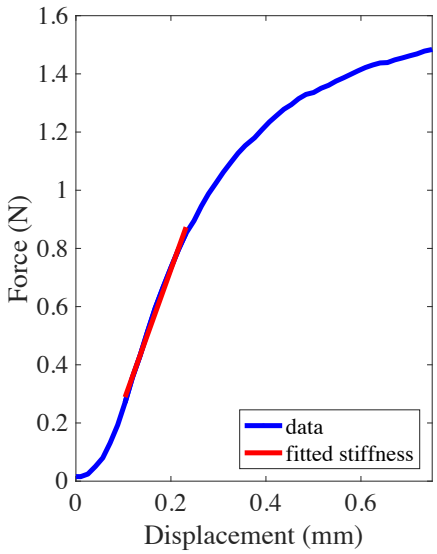

Fig. 4-1 Section of the force-displacement curve for a specimen in the MD, corresponding to the blue force-displacement curve in the MD in **Fig. 3-1**b. Prior to 0.1 mm, the curve was nonlinear; after 0.1 mm, it was linear and was used for the stiffness fit (red line).

The measurements were similar to previous studies of single bonds. Bhat et al. [13] reported the peak loads from the single bond pure polypropylene uniaxial strip test in the MD. Comparatively, the results from the current work on biaxial single bond tests found loads on the same magnitude, though slightly higher.

Using the same nonwoven material, uniaxial tests were also performed (Appendix B). Similar specimen preparation was performed, except the specimens were unidirectional bowtie shaped specimens, oriented either in the MD (n = 10) or CD (n = 10), and fibers that were not part of the bond were cut to prevent them from carrying load. Specimens were uniaxially tensile tested at 0.1 mm/s. The average maximum force in the MD and CD were 0.429 ± 0.089 N and 0.116 ± 0.050 N, respectively. Similar to the biaxial tensile tests, the maximum force in the MD was higher than in the CD. However, in both the MD and CD, the maximum forces were lower in the uniaxial tests compared to the biaxial tests. This can likely be attributed to the specimen preparation. For the uniaxial tests, extraneous fibers that did not directly affect the bond were cut, but for biaxial tests, those fibers were not cut and could have continued to carry a portion of the load (Fig. 3-8b).

There was a significant variation in the non-scaled data collected in the MD and the CD (Fig. 3-3 and Fig. 3-5) and within each individual direction (Fig. 3-2). However, by taking into account the relative basis weight, orientation of the fibers surrounding the bond, and width of the bond, the variation was reduced to where there was no statistically significant difference detected between the stiffness and maximum force in the MD and the CD (Fig. 3-7). Initial attempts were made to scale the maximum force and stiffness using the relative basis weight and orientation only. Such preliminary scaling, similar to previous thermomechanical bond research [28], reduced the difference in the MD and CD of the maximum force (from $p = 1.1\times10^{-7}$ to $p = 0.122$) and stiffness (from $p = 2.05\times10^{-9}$ to $p = 0.008$). However, since previous studies noted that nonwoven uniaxial tensile properties were similar in the MD and CD when measuring force per unit width [16], the data in the MD and CD were further scaled by the width of the bond in the corresponding direction.

This further reduced the differences in the MD and CD of the maximum force ($p = 0.884$) and stiffness ($p = 0.144$). In the future, variation in the mechanical behavior of the bonds can be further reduced by taking into account the fiber orientation and bond width through the duration of the test. For example, the images being collected for strain measurement purposes in this study could also be used to measure fiber orientation and bond width using ImageJ and an orientation parameter and bond width based on the current configuration could be calculated. Caution is, however, necessary when measuring the bond width during testing due to the possible formation of voids. It must also be noted that this study focused on selecting bonds with similar relative basis weights. Future work should verify that the scaling proposed here can be extended to bonds in nonwoven having a variety of basis weights.

Through the captured images (Fig. 3-8), all bonds were seen nominally disintegrating into the individual fibers that originally formed them. The fibers used for the nonwoven were bi-component, composed of a polyethylene sheath and polypropylene core, and were thermomechanically bonded at discrete points. The temperature at which these bonds were formed was likely high enough to melt the polyethylene of the sheath, but not the polypropylene of the core. Therefore, when the bonds were pulled in tension, the fused polyethylene film likely broke, but the polypropylene fibers still held their original shape. While the bonds consistently experienced the same failure mode in the biaxial tests, this was not always the case for the uniaxial tests (Appendix B). In some specimens subjected to uniaxial tests, the bond was observed to tear and in other specimens, very minimally deform. One cause for this discrepancy in failure mode is the specimen preparation method. When selecting specimens to uniaxially test, the basis weight was not taken into

account. Therefore, it is possible that specimens with a low basis weight were tested uniaxially and those specimens perhaps did not have enough fibers to form complete bonds, and instead had bonds filled with voids. Furthermore, specimens with low basis weights may not always have enough fibers in the loading direction to transfer load to the bond and, therefore, the bond did not experience much damage and instead fiber failure occurred. On the other hand, the basis weight that was chosen for biaxial tests featured bonds that were complete, with minimal voids. Additionally, by testing biaxially, enough fibers were present to transfer load to the bond in at least one of the loading directions.

While the specimens were equally displaced in both the MD and CD, the strain experienced by the individual bonds was not equal in these directions. The strain was always positive in the MD but it was often negative in the CD (Fig. 3-9). One cause could be an insufficient number of fibers in the CD. The fibers being pulled in the MD cause the bond to collapse in the CD and therefore the bond experienced negative strain in the CD. Fluctuations between increases and decreases in the strain were likely caused by the fibers straightening out and becoming load bearing and/or by fiber breakage. Kim et al. previously reported the variation in strain response of single bonds. While the study tested coupons of nonwovens with multiple bonds, strain measurements were performed on single bonds and the strain experienced would vary from increasing to decreasing [29]. Future tests can be performed at higher displacement rates in the CD than in the MD, rather than at equal displacement rates in the two directions, in order to generate positive strain in the CD.

Strain measurements were also performed on the uniaxial tensile tests (Appendix B). Unlike the biaxial tests, the uniaxial tests suggested a Poisson effect, where the bond

experienced positive strain in the loading direction (either in the MD or CD) and negative strain perpendicular to the loading direction, similar to that of Fig. 3-9c. There were also cases in the uniaxial tests where the bonds experienced minimal strain (<5%), though this was not seen in the biaxial tests. This lack of strain could be caused by an insufficient number of fibers transferring load into the bond. On the other hand, by testing both directions simultaneously in the biaxial tests, there were always enough fibers to transfer load to the bond in at least one direction.

The calculated strain data were correlated to the measured force rather than the stress (Fig. 3-9). The Cauchy stress, the stress relative to the current configuration, could not be determined due to difficulties measuring the changing thickness of the specimen during testing. It must be noted that, in previous uniaxial tensile studies of polypropylene nonwoven samples, the strain was presented as a function of a "nominal tensile stress," which was calculated by dividing the force by the initial width [17]. This "nominal tensile stress" could be computed in the present work; however, since the Eulerian strain was calculated, it would be more appropriate to divide the force by the width in the current configuration.

By utilizing the DIC method, the local and average strains of the bonds were calculated. However, the application of this method to nonwovens had limitations. Typically for DIC, several tracking points are aligned to evenly spaced grid. However, for our specimens, the tracking points were manually selected due to the inability to achieve sufficiently dense speckle patterns and because individual tracking points often disappeared or dislodged from the bond, especially when fibers were pulled out of the bond. The fibers also occasionally moved over the plane containing the bond, obstructing the view and

preventing points on the bond from being tracked. The fiber straightening also caused speckles near the border of the bond to disappear and thus these points could not be tracked. Due to these limitations, the strain map at the border of the bond could not be obtained (Fig. 3-10 and Fig. 3-11). The average strain was analyzed up to a set displacement (from 0.0 mm up to 2.3 mm) because, after this displacement, too much damage or movement of the speckles within the bond occurred and the speckles could not be readily tracked. Although automated DIC analysis is robust for continuous materials, the complexity of the nonwoven bond sites made the analysis process tedious and time consuming. Images of the specimens had to be carefully analyzed to find speckles that were consistently visible and could be successfully tracked. Even then, the open-source DIC program was not robust enough to always accurately detect and track the desired speckles.

This work provides insight into the biaxial behavior of individual bonds, which to the researcher's knowledge, has not previously been studied. Knowledge of the biaxial tensile behavior of individual bonds in nonwovens could enable manufacturers to make more informed decisions about producing or selecting nonwoven materials and their the ultimate applications. By developing an understanding of the individual bonds and surrounding fibers, the behavior of the nonwoven as a whole can be better understood. While this experimental study focuses on the bond width, orientation of surrounding fibers, and relative basis weight of a single commercial nonwoven fabric, the testing techniques developed can be extended to other nonwoven fabrics, including those made with a variety of processing parameters, such as bonding temperature and fiber composition.

Chapter 5. Conclusions

This study developed a method to examine the equi-biaxial response of individual bonds from a thermomechanically bonded nonwoven fabric. Specimens were prepared and oriented such that the MD and CD of the nonwoven were tested. Equi-biaxial tests were performed at 0.1 mm/s and images were captured through the duration of the test. Analysis of the raw force and displacement data showed that specimens had higher maximum force and stiffness in the MD than in the CD. Student's t-tests revealed that the difference in the CD and in the MD was statistically significant for both the maximum force and stiffness. Scaling the maximum force and stiffness by the relative basis weight, orientation parameter, and width of the bond reduced the difference in the two directions to no statistical significance. This indicates that the biaxial response is dependent on these factors. The bonds in the specimens were consistently observed to disintegrate and nominally return to their original, individual fiber form. This was attributed to the fiber's bi-component composition and the temperature at which the bonds were formed. It is assumed that the temperature at which the bonds were formed was high enough to melt the polyethylene and form the bond but not high enough to melt the polypropylene and therefore it was able to keep its original structure. DIC was utilized in order to measure the strain experienced by the bond. Strains in the MD were consistently positive and increasing while strains in the CD varied from increasing to decreasing. This variation was likely dependent on the number of fibers in each direction. The strain response in the CD was dependent on the fibers Strain maps of the local strains displayed the inhomogeneity experienced within bonds. Knowledge of individual bonds in nonwoven fabrics can be used

to better understand the fabrics as a whole, as well as better tailor them to their final application.

References

1. Russell, S.J. and I. Textile, *Handbook of nonwovens*. 2007, Boca Raton, Fla;Cambridge;: CRC Press.
2. Dasdemir, M., B. Maze, N. Anantharamaiah, and B. Pourdeyhimi, *Influence of polymer type, composition, and interface on the structural and mechanical properties of core/sheath type bicomponent nonwoven fibers.* Journal of Materials Science, 2012. **47**(16): p. 5955-5969.
3. Wust, J.C.J., *Fibers, Olefin*, in *Kirk-Othmer Encyclopedia of Chemical Technology*. 2000, John Wiley & Sons, Inc.
4. Kittelmann, W., J.P. Dilo, V.P. Gupta, P. Kunath, J. Schreiber, A. Wegner, W. Zäh, U. Münstermann, W. Möschler, A. Watzl, and P. Böttcher, *Web Bonding*, in *Nonwoven Fabrics*. 2005, Wiley-VCH Verlag GmbH & Co. KGaA. p. 269-408.
5. Kim, H.S., *Relationship between fiber orientation distribution function and mechanical anisotropy of thermally point-bonded nonwovens.* Fibers and Polymers, 2004. **5**(3): p. 177.
6. Demirci, E., M. Acar, B. Pourdeyhimi, and V.V. Silberschmidt, *Finite element modelling of thermally bonded bicomponent fibre nonwovens: Tensile behaviour.* Computational Materials Science, 2011. **50**(4): p. 1286-1291.
7. Sozumert, E., F. Farukh, E. Demirci, M. Acar, B. Pourdeyhimi, and V.V. Silberschmidt. *Damage mechanisms of random fibrous networks*. in *Journal of Physics: Conference Series*. 2015. IOP Publishing.

8. Farukh, F., E. Demirci, B. Sabuncuoglu, M. Acar, B. Pourdeyhimi, and V.V. Silberschmidt, *Mechanical analysis of bi-component-fibre nonwovens: Finite-element strategy.* Composites Part B: Engineering, 2015. **68**: p. 327-335.

9. Gao, X. and L. Wang, *Finite element modelling for tensile behaviour of thermally bonded nonwoven fabric.* Autex Research Journal, 2015. **15**(1): p. 48-53.

10. Wang, H., X. Jin, N. Mao, and S. Russell, *Differences in the tensile properties and failure mechanism of PP/PE core/sheath bicomponent and PP spunbond fabrics in uniaxial conditions.* Textile Research Journal, 2010. **80**(17): p. 1759-1767.

11. Nanjundappa, R. and G.S. Bhat, *Effect of processing conditions on the structure and properties of polypropylene spunbond fabrics.* Journal of Applied Polymer Science, 2005. **98**(6): p. 2355-2364.

12. Kim, H., B. Pourdeyhimi, P. Desai, and A. Abhiraman, *Anisotropy in the mechanical properties of thermally spot-bonded nonwovens: experimental observations.* Textile Research Journal, 2001. **71**(11): p. 965-976.

13. Bhat, G.S., P.K. Jangala, and J.E. Spruiell, *Thermal bonding of polypropylene nonwovens: Effect of bonding variables on the structure and properties of the fabrics.* Journal of Applied Polymer Science, 2004. **92**(6): p. 3593--3600.

14. Goswami, B.C., J. Suryadevara, and T.L. Vigo, *Determination of Poisson's Ratio in Thermally Bonded Nonwoven Fabrics.* Textile Research Journal, 1984. **54**(6): p. 391-396.

15. Zhang, D. and D.D. Arola, *Applications of digital image correlation to biological tissues.* Journal of Biomedical Optics, 2004. **9**(4): p. 691-699.

16. Jubera, R., A. Ridruejo, C. González, and J. Llorca, *Mechanical behavior and deformation micromechanisms of polypropylene nonwoven fabrics as a function of temperature and strain rate.* Mechanics of Materials, 2014. **74**: p. 14-25.

17. Ridruejo, A., C. González, and J. Llorca, *Failure locus of polypropylene nonwoven fabrics under in-plane biaxial deformation.* Comptes Rendus Mécanique, 2012. **340**(4): p. 307-319.

18. Ridruejo, A., R. Jubera, C. González, and J. LLorca, *Inverse notch sensitivity: Cracks can make nonwoven fabrics stronger.* Journal of the Mechanics and Physics of Solids, 2015. **77**: p. 61-69.

19. Morison, P.M., R. Chhabra, D.P. Gruenbacher, D.W. Monebrake, and S.L. Wilking, *Method of filtering particulates from the air using a composite filter substrate comprising a mixture of fibers*. 2016, Google Patents.

20. Chhabra, R., D.P. Gruenbacher, D.W. MONEBRAKE, P.M. MORISON, and S.L. WILKING, *Composite filter substrate comprising a mixture of fibers*. 2016, Google Patents.

21. Eberl, C., R. Thompson, D. Gianola, W. Sharpe Jr, and K. Hemker, *Digital image correlation and tracking.* MatLabCentral, Mathworks file exchange server, FileID, 2006. **12413**.

22. Sage, D., *OrientationJ: ImageJ's plugin for directional analysis in images*. 2012.

23. Püspöki, Z., M. Storath, D. Sage, and M. Unser, *Transforms and Operators for Directional Bioimage Analysis: A Survey*, in *Focus on Bio-Image Informatics*, W.H. De Vos, S. Munck, and J.-P. Timmermans, Editors. 2016, Springer International Publishing: Cham. p. 69-93.

24. Cox, H.L., *The elasticity and strength of paper and other fibrous materials.* British Journal of Applied Physics, 1952. **3**(3): p. 72.

25. Jacobs, N.T., D.H. Cortes, E.J. Vresilovic, and D.M. Elliott, *Biaxial tension of fibrous tissue: using finite element methods to address experimental challenges arising from boundary conditions and anisotropy.* Journal of biomechanical engineering, 2013. **135**(2): p. 021004.

26. Beccarelli, P., *Biaxial testing for fabrics and foils: Optimizing devices and procedures*. 2015: Springer.

27. Nolan, D. and J. McGarry, *On the correct interpretation of measured force and calculation of material stress in biaxial tests.* Journal of the mechanical behavior of biomedical materials, 2016. **53**: p. 187-199.

28. Rittenhouse, J., *Deformation and Fracture Behavior of Thermomechanical Bonds in Nonwoven Fabrics*, in *Department of Materials Science and Engineering*. 2016, Virginia Polytechnic Institute and State University.

29. Kim, H.S., A. Deshpande, B. Pourdeyhimi, A.S. Abhiraman, and P. Desai, *Characterizing Structural Changes in Point-Bonded Nonwoven Fabrics During Load-Deformation Experiments.* Textile Research Journal, 2001. **71**(2): p. 157-164.

Appendix A. Average Strain Sensitivity Analysis

In order to ensure that the average strain determination was truly representative of the specimen, attempts were made to remove and/or add points to be tracked in order to observe the change in resulting strain. The desired outcome was that the addition or removal of the tracking points would minimally affect the resulting strain. For the specimen shown in Fig. A-1, the average strain in the MD and CD are calculated using 3, 4, and 5 tracking points. There is minimal difference between the e_{xx} strains, and while there is some variation in the e_{yy} strain, it can be noted that the strain values are relatively small (-2 to +2%) compared to the strains experienced in the MD (~40%).

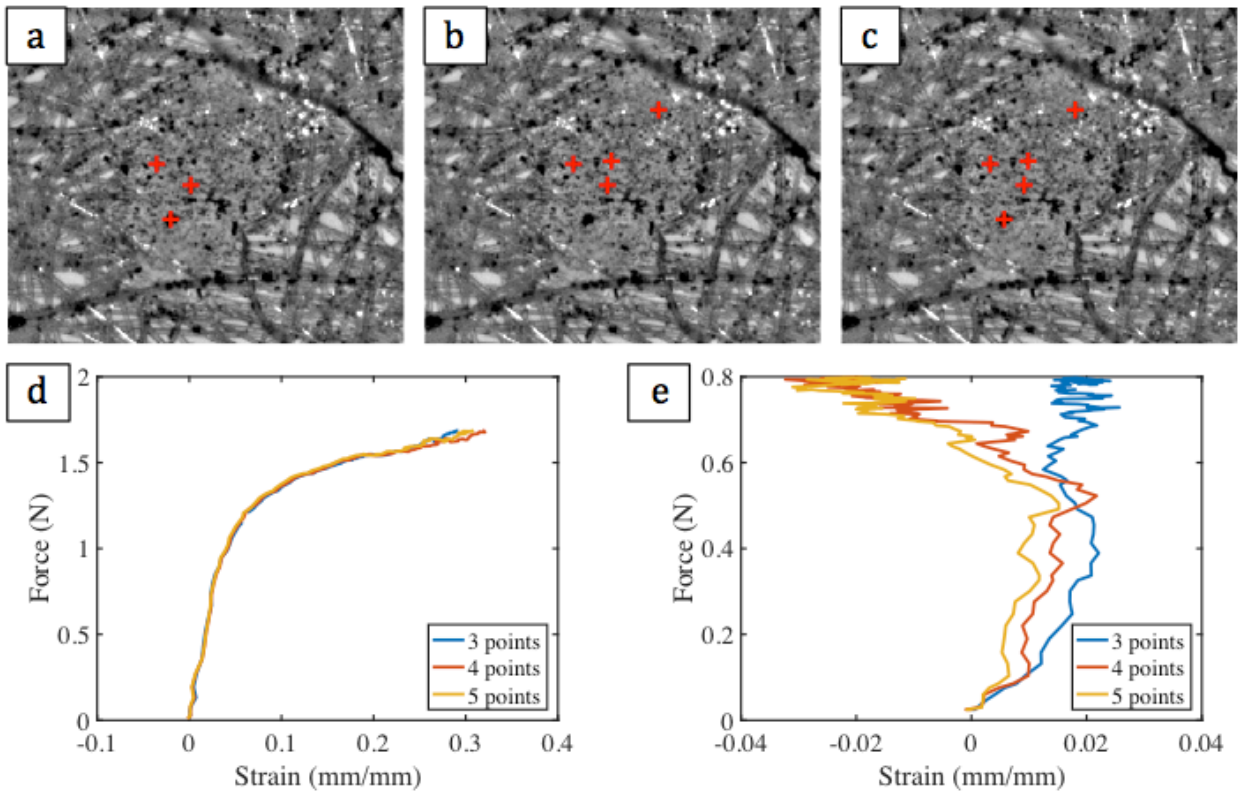

Fig. A-1 Average strains based on (a) 3 tracking points, (b) 4 tracking points, and (c) 5 tracking points for a specimen (d) in the MD ($\boldsymbol{e_{xx}}$) and (e) in the CD ($\boldsymbol{e_{yy}}$).

A second specimen further shows the insensitivity to chosen points. Average strains were calculated using 4, 5, and 6 tracking points. Force vs. strain in the MD and CD are plotted in Fig. A-2. The addition of the tracking points minimally affects the average strain in both the MD and CD. This verification method was repeated for other specimens, though not presented.

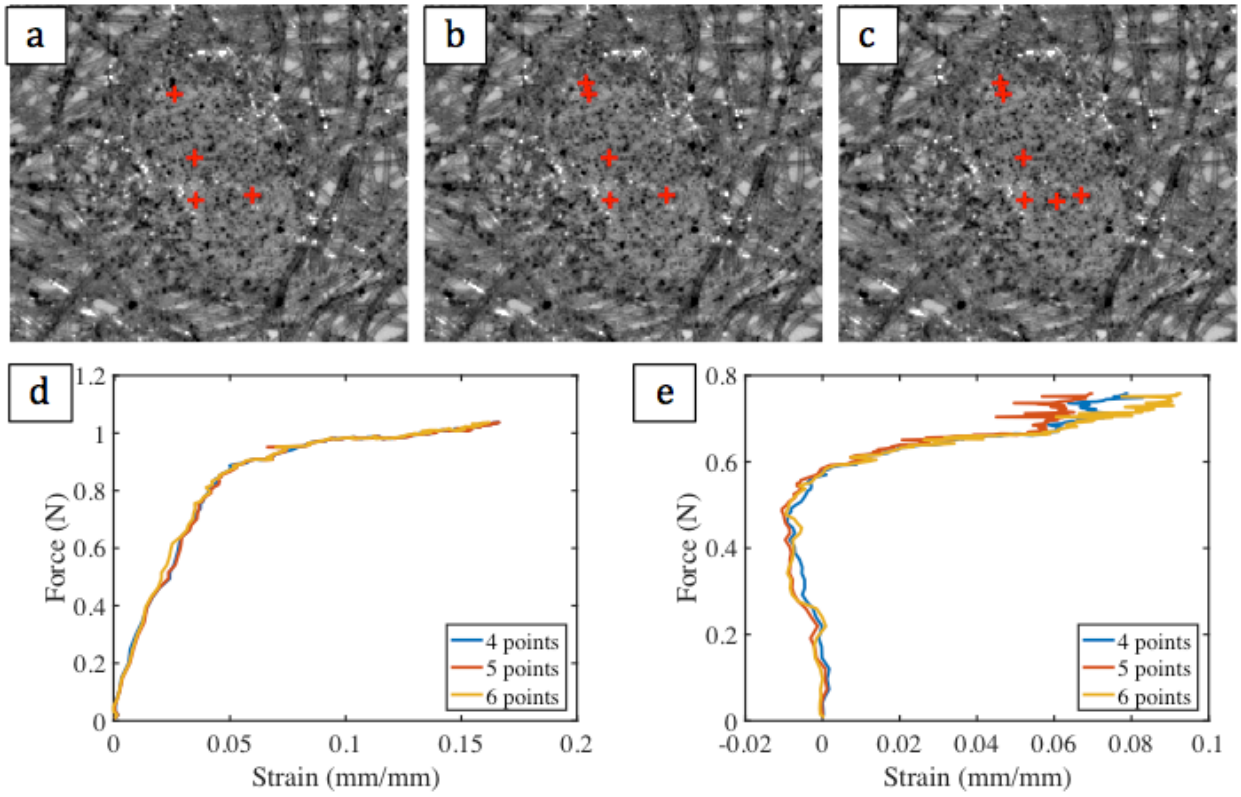

Fig. A-2 Average strains based on (a) 4 tracking points, (b) 5 tracking points, and (c) 6 tracking points for a specimen (d) in the MD ($\boldsymbol{e_{xx}}$) and (e) in the CD ($\boldsymbol{e_{yy}}$).

Appendix B. Uniaxial Tests

B.1. Methods

The same commercially available nonwoven fabric used for the biaxial tensile tests was used for uniaxial tensile tests. Methods for tensile testing bonds uniaxially were developed from Rittenhouse [28]. The fabric was laser-cut into 100 bowtie oriented in the MD and 100 bowties oriented in the CD. The laser only cut the portion of the specimen that was mounted and clamped. Fig. B-1 shows the uniaxial bowtie specimen geometry.

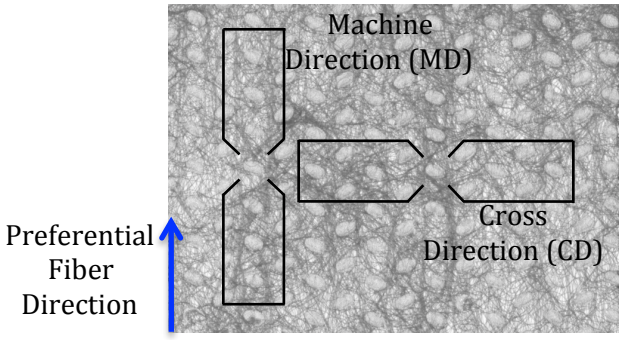

Fig. B-1 Uniaxial bowtie specimen design for testing in the MD and CD. The black lines indicate the region that was laser cut.

While 200 bowties were cut, only bowties with bonds located in the center were used for tensile testing; basis weight and the orientation parameter were not used as a metric for choosing bonds to be tested. The laser-cut fabrics were scanned to allow for additional analysis. Once bowties were chosen for testing, remaining cuts were done using micro-scissors. Similar to the biaxial mounting method, the bowties were adhered to plastic mounting frames (Gridded Template Plastic, Dritz Quilting) using double-sided PSA. The plastic frame had a 2 *mm* wide gap for the bond to be centered over. An epoxy was applied to secure the arms of the bowtie to the mounting frame. Within the 2 *mm* gap, fibers that

did not directly enter the bond were cut. A random speckle pattern was then applied to the specimen using an airbrush with India ink. A prepared bowtie specimen is shown in Fig. B-3

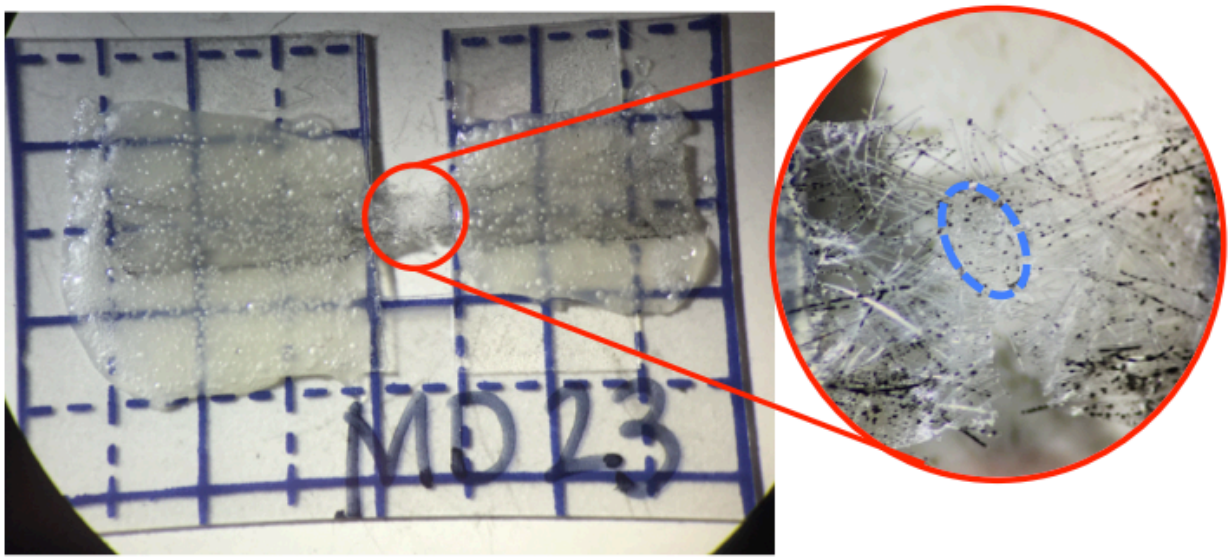

Fig. B-2 A speckled bowtie specimen attached to the plastic mounting frame using double sided PSA and epoxy. Dashed blue line shows the approximate location of the individual bond to be tested.

The uniaxial tensile testing stage featured two linear actuators (Linear actuator, 25 mm travel, RS-232 plus manual control, Zaber Technologies Inc.) to control the position of the specimen along one direction, an 8.9 N (2 lb.) load cell (Jr. Miniature S-Beam Load Cell, FUTEK Advanced Sensor Technology, Inc.), mechanical clamps, and an XGA camera (Stingray F-080, Allied Vision Technologies) attached to a microscope (M3Z, Leica Wild). A LabVIEW program written to control the actuators, load measurement from the load cell, and image acquisition. Manual controllers within this program were designed to allow the user to keep the bonds centered in the field of view during testing.

The specimen was mounted into the tensile testing stage. The plastic mounting frame was cut to allow movement along the 2 mm spacing. The specimen was pre-loaded to 0.01

N prior to testing. The test was performed at room temperature (20°C) at a constant 0.1 mm/s displacement rate on the specimens (n = 10 in the MD and n = 10 in the CD). The tests were run until either specimen failure occurred or an actuator's physical limit was reached.

Upon completion of the test, strain and statistical analysis were performed on the uniaxial data following the biaxial methods.

B.2. Results

The force-displacement curves for the specimens tested in the MD and CD are plotted in Fig. B-3. The average maximum force in the MD was 0.429 ± 0.089 N and occurred at an average displacement of 6.33 ± 1.07 mm. The average maximum force in the CD was 0.116 ± 0.050 N and occurred at an average displacement of 3.60 ± 1.62 mm. The difference between the maximum forces reached in the MD compared to the CD was statistically significant ($p = 5.01 \times 10^{-6}$).

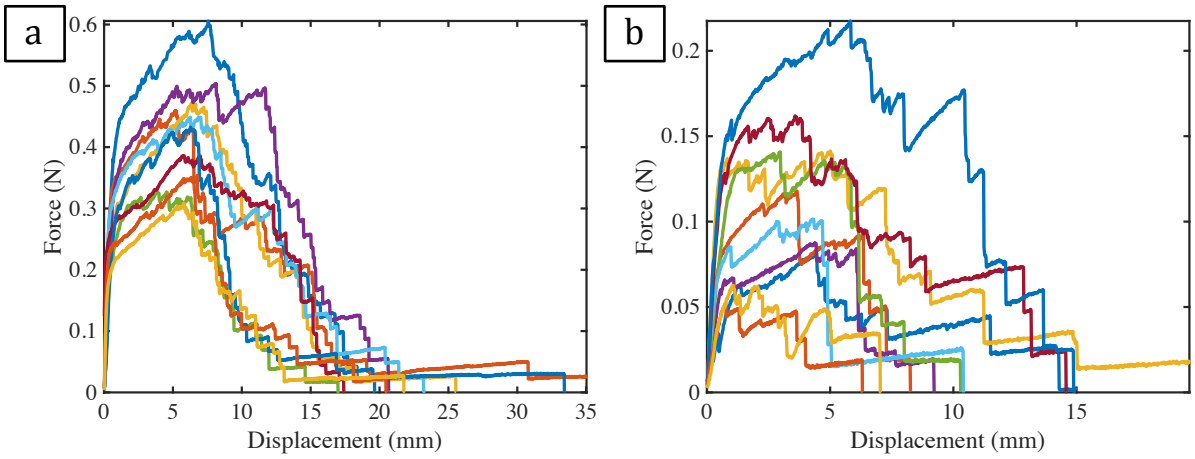

Fig. B-3 Force-displacement curves for the specimens (a) in the MD (n = 10) and (b) in the CD (n = 10).

Images of the uniaxial tests revealed a variety of bond responses when pulled in tension. In some cases, the bonds stay perfectly intact through the duration of the test and

did not fail, as shown in Fig. B-4. Other specimens experienced tear propagation, which could sometimes be attributed to voids within the bond, like in Fig. B-5. The remaining bond fragments were in contrast to the biaxial tests, where bond disintegration was observed. It was also seen that the complete bond did not always remain visible. For example, a portion of the bond in the specimen presented in Fig. B-6 folded and formed a pleat towards the beginning of the test.

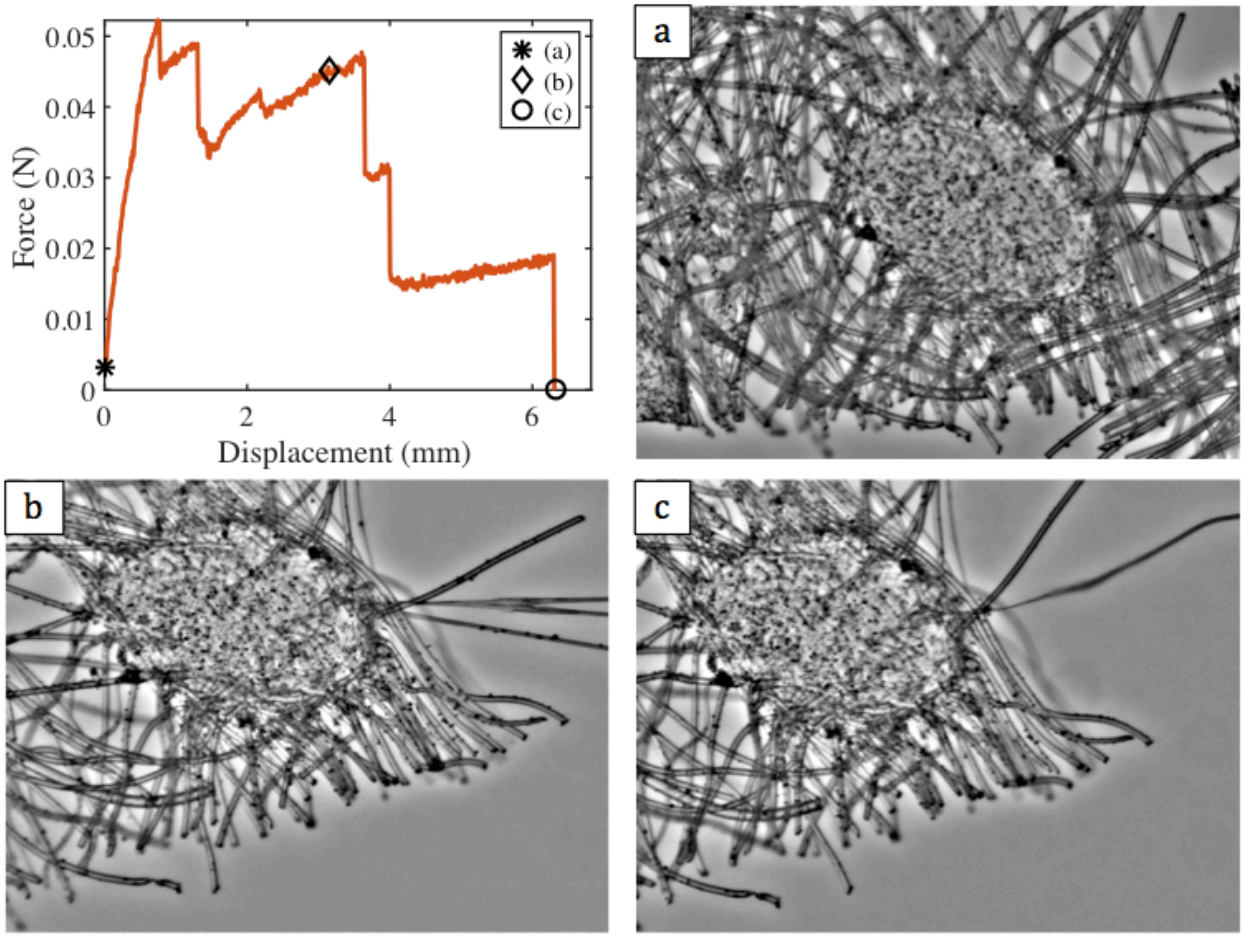

Fig. B-4 A bond in a specimen oriented in the CD did not show damage and no strain was detected visually at loads of (a) 0.003 N, (b) 0.045 N, and (c) 0 N (specimen failure).

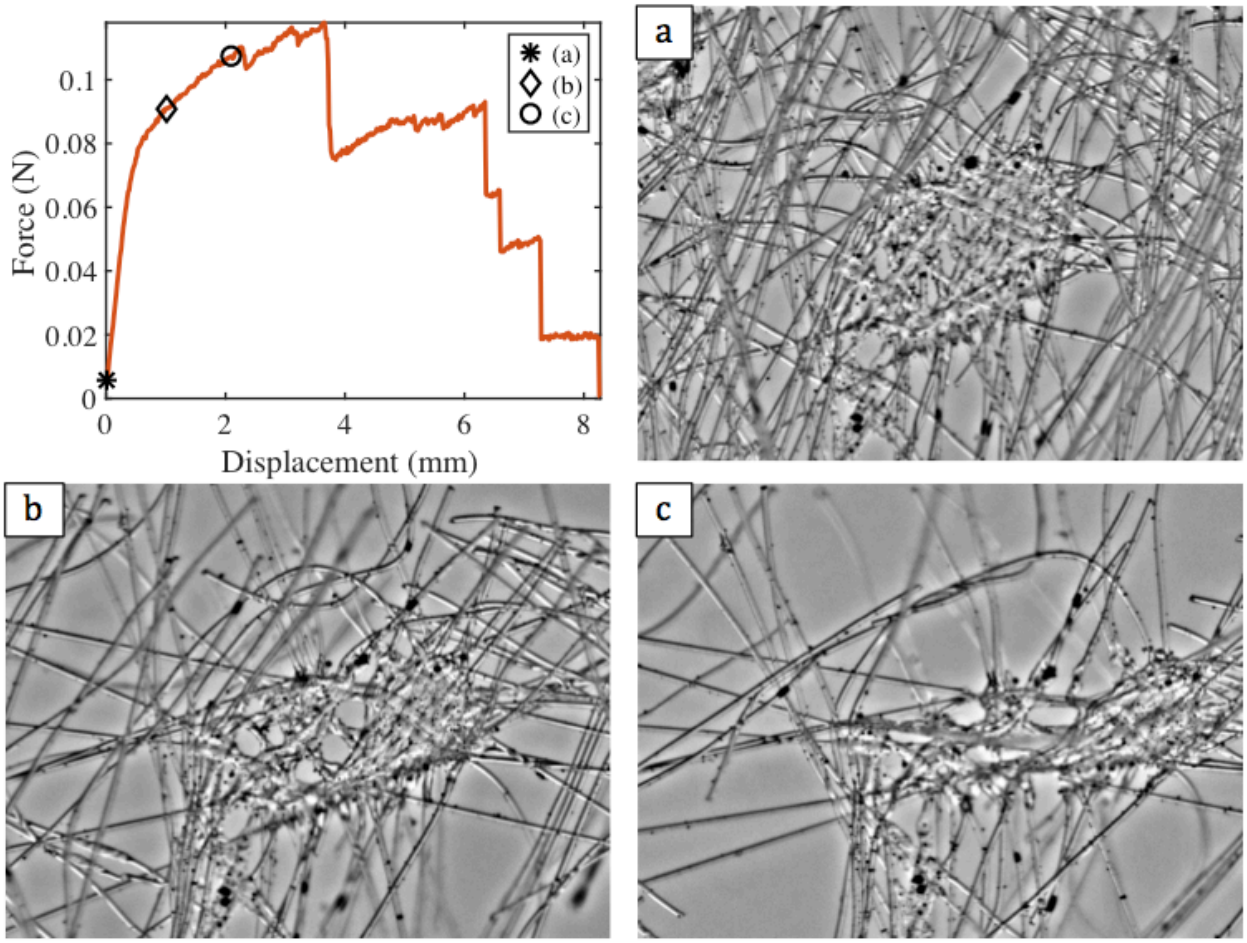

Fig. B-5 A bond in a specimen oriented in the CD with initial voids within the bond. These voids grew and caused the bond to tear. Image sequence is at loads (a) 0.007 N, (b) 0.091 N, and (c) 0.107 N.

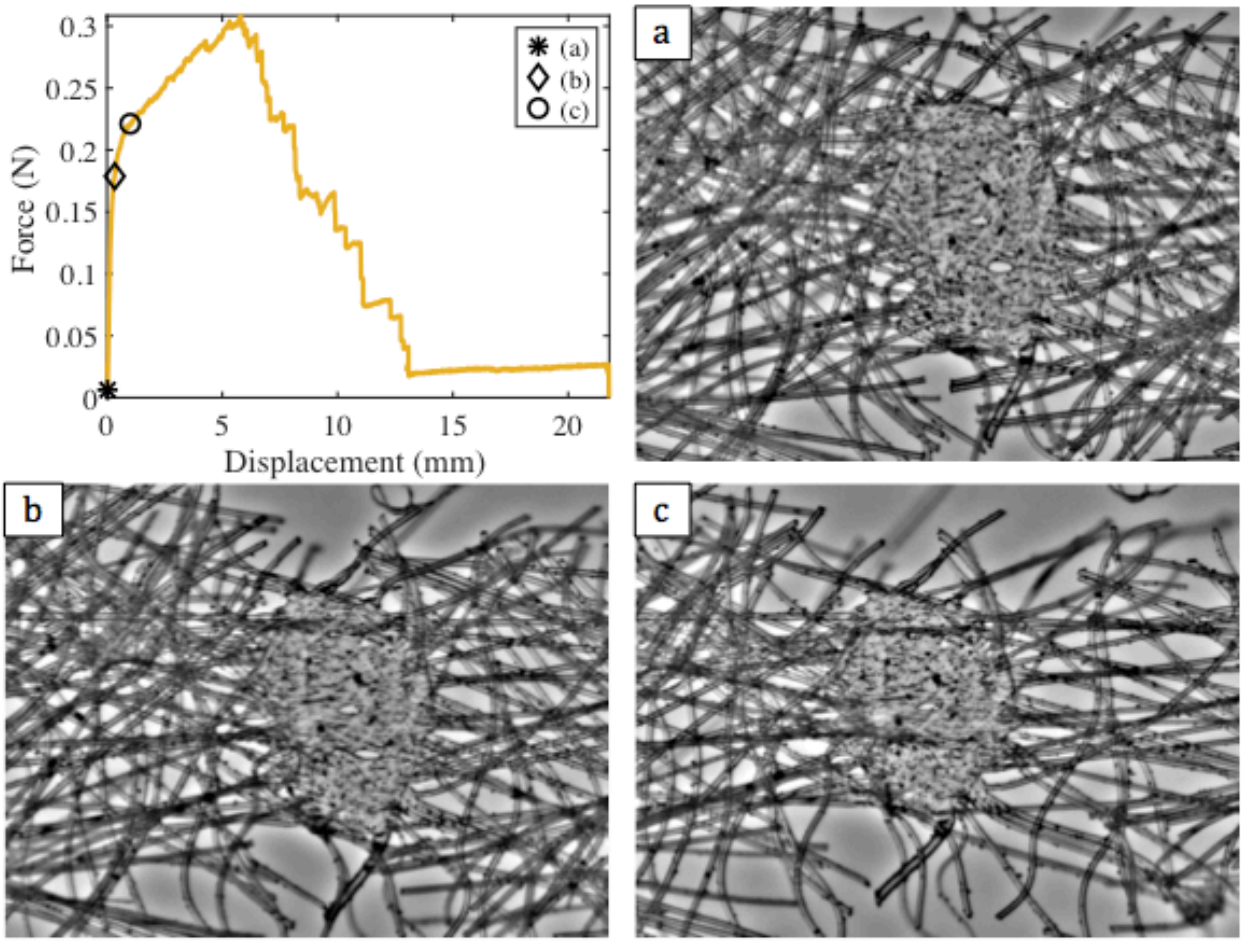

Fig. B-6 A bond in a specimen oriented in the MD experienced folding during the initial portion of the test, at loads of (a) 0.008 N, (b) 0.179 N, and (c) 0.221 N.

Strain analysis was also performed on the uniaxial tests. Some bonds were seen to experience a Poisson effect, where the strain in one direction (i.e. the loading direction) would increase while the strain in the other direction (i.e. perpendicular to the loading direction) would decrease (Fig. B-7). In other cases, the bonds would experience very minimal strain (<5%), as plotted in Fig. B-8.

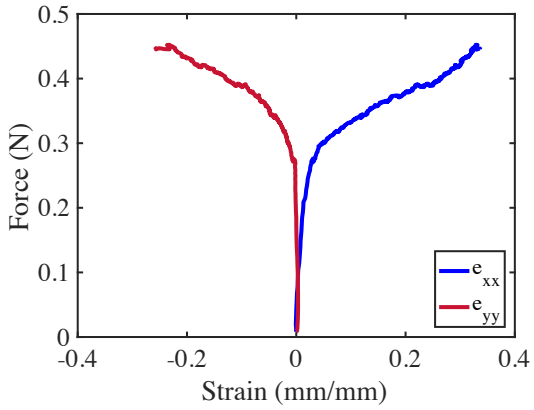

Fig. B-7 Force vs. strain curves for a bond in specimen oriented in the MD. $\boldsymbol{e_{xx}}$ corresponds with the loading direction (in the MD), while $\boldsymbol{e_{yy}}$ corresponds with perpendicular to the loading direction

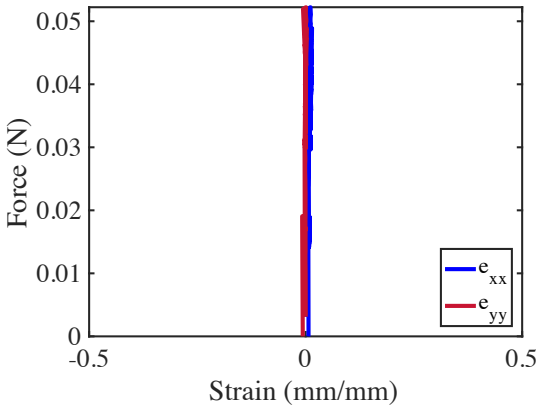

Fig. B-8 Force vs. strain curves for a bond in a specimen oriented in the CD (**Fig. B-4**). $\boldsymbol{e_{xx}}$ corresponds with the loading direction (in the CD), while $\boldsymbol{e_{yy}}$ corresponds with perpendicular to the loading direction. Even with changes in load, the bond experienced minimal strain.